EVALUATING DEVELOPMENTAL SHAPE SELECTIVITY FROM SIMULTANEOUS MULTI-UNIT RECORDINGS ALONG THE VENTRAL VISUAL PATHWAY

A Dissertation
Presented to
The Academic Faculty

By

Andrew Ezra Sutter

In Partial Fulfillment
of the Requirements for the Degree
Bachelor of Science in the
College of Liberal Arts
Department of Neuroscience

Drew University

May 2023

EVALUATING DEVELOPMENTAL SHAPE SELECTIVITY FROM SIMULTANEOUS MULTI-UNIT RECORDINGS ALONG THE VENTRAL VISUAL PATHWAY

Thesis committee:

Dr. Christina McKittrick
Biology
Drew University

Dr. Graham Cousens
Psychology
Drew University

Dr. Steve Kass
Mathematics and Computer Science
Drew University

Date approved: May 18, 2023

Abstract

Neurons of cortical area V4 are selective for shape – the conformation of contrast boundaries that outline objects in a visual scene. However, it is unknown how this selectivity arises in the ventral visual pathway, and whether shape tuning depends on visual experience in early life. To answer these questions, the Visual Neuroscience Laboratory (VNL) at New York University implanted 96-channel "Utah" electrode arrays in areas V2 and V4 of two fixation-trained juvenile *Macaca nemestrina*. VNL recorded neural responses to shape stimuli with a single parametrically-varied curvature component (El-Shamayleh and Pasupathy, 2016), at both 7 and 12 months of age in macaques which translates to approximately an age of 2.5 and 4.3 human years (Kiorpes, 2016).

To assess curvature selectivity we fit neural responses with the Angular Position and Curvature (APC) model (Pasupathy and Connor, 2001). We found that it explained the response variance ($r^2 > 0.1$) of many sites in both V2 (74% of n = 64) and V4 (75% of n = 95). Interestingly, we found that a simple image-computable model based on reverse correlation of local stimulus luminance could explain most sites in V2 (97%) and V4 (93%). 1% and 5% of sites (V2 and V4, respectively) were unexplainable by either model.

To account for experimental differences between our work and prior studies, we performed control analyses using a previously-published dataset of well-isolated shape-selective V4 neurons (Pasupathy and Connor, 2001). We quantified our ability to characterize the selectivity of simulated multi-unit responses with an expanded shape set, and of single-unit responses with a range of shape stimuli chosen to match our experimental conditions. Collectively, these results support our observation of shape selectivity in ventral visual areas of the juvenile macaque. A comparison of model fits across developmental age points suggest that V2 and V4 sites are well-tuned for shape features from the earliest ages tested.

TABLE OF CONTENTS

LIST OF FIGURES

CHAPTER 1

INTRODUCTION

The visual system is a complex and critical component of an organism's ability to perceive and interpret the surrounding environment. Vision plays a crucial role in navigating the environment as well as detecting and identifying objects. Largely, the visual system contains interconnected neural circuits and pathways that process and extract information about a visual scene. Starting at the eye, the cornea and the lens focus light onto the retina, containing specialized light-sensitive cells, at the back of the eye. These cells capture light energy and convert it into electrical signals that are transmitted to the brain via the optic nerve.

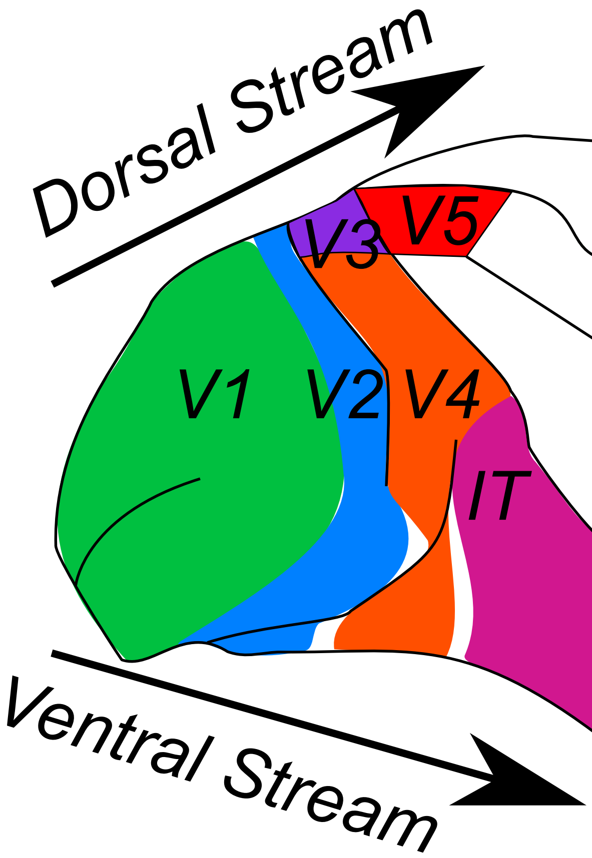

Figure 1.1: A schematic of the brain and several visual areas. The dorsal and ventral streams are labeled.

The visual section of the brain contains several functional areas: V1, V2, V4, IT, V3, and V5, to name a few. V1 is known to be selective for oriented bars of varying widths and lengths. V2 is known to be selective for textures, motion, and spatial frequency. V4 is selective for color and shape and IT is responsive to complex shapes, objects, and faces. In contrast, V3 and V5 are selective for motion processing, depth perception, and spatial processing. Due to the functional differences between the areas, researchers assigned the areas to different processing pathways called the dorsal and ventral streams.

The dorsal stream is also referred to as the "where" or "action" pathway and is responsible for processing related to spatial location, motion, depth, navigation, and motor planning. Visual areas

V2, V3, and V5 belong to this processing stream due to the overlap of the selectivity preferences. The ventral stream also known as the "what" pathway processes information about shape, color, and object identity and includes V2, V4, and IT. Both the dorsal and ventral pathways start in the primary visual cortex (V1) and diverge after area V2. While the dorsal stream heads toward the top of the brain, the ventral stream travels along the bottom edge of the brain. Despite the separation of these pathways, they both play an integral role in an organism's ability to perceive and make sense of the visual world.

Overall, vision is a remarkable example of the capability of the nervous system. A nuanced understanding of the processing that occurs within and between functional areas is important for many clinical and technological applications aimed to improve quality of life for those with visual dysfunctions. Subsections of this introduction will cover the processing within the visual system, developmental visual disorders, and visual development in more detail.

1.1 The visual system- an overview

The visual system is crucial for providing an intimate understanding of and interaction with our environment. By tracing the generation of signals from a stimulus within our visual world to higher-level visual cortex, we can gain insight and an appreciation for the visual system and its complexity. For further reading on the visual system see Bear et al. (2016) chapters 9 and 10.

1.1.1 The eye

Throughout the day, the eyes are constantly jumping from one location in visual space to another. Known as saccades, these eye movements are crucial for focusing an object's image correctly on the retina, a thin layer of cells that are responsible for the detection of a visual stimulus. To briefly explain some key components of the visual system related to object recognition, we will trace the resulting processing caused by a saccade to a dog.

Photons are either reflected or emitted from a stimulus which allows for our perception of the stimulus. However, in the case of the dog, the photons that contact the retina are originally reflected and may come in contact with the cornea, a thin lens-like structure that lies on the outermost surface of the eyeball. This particular structure, with the aid of several others, directs the incoming light toward the retina. Since the cornea cannot bend and change its shape, it is unable to alter the refractive power, but there are other more malleable structures that aid in ensuring proper focusing of light in healthy eyes.

The most important contributing structure to the image formation of the dog on the retina is the lens. Long transparent cells bundled together form the biconvex structure and allow for focusing of light. Ciliary muscles surround the lens and manipulate the thickness to alter the refractive power so that light can be optimally converged at the retina to create a clear image. As a viewed object moves away from the eye, a lesser refractive power is necessary to bend the light onto the retina, and therefore a graded change in the contraction of the ciliary muscles is necessary to decrease the curvature of the lens. The contraction is typically simultaneous in time and strength in both eyes.

The section Amblyopia: causes, treatments, and implications will discuss amblyopia, a visual development disorder in more depth. As mentioned in that section, one risk factor for amblyopia is anisometropia, which refers to differences in refractive powers in both eyes. The refractive difference can stem from dissimilar stiffnesses of the lenses, different lengths of the eyeballs, or different refractive powers of the corneas between the two eyes.

In normal visual function, the lens refracts light onto the retina allowing for the initiation of visual function. The back of the retina consists of photoreceptors, either rods or cones, that have different spatial densities. The cones are largely concentrated within the fovea, a small indented region on the retina, and allow for high acuity and color vision. Additionally, this region processes light that travels from a viewer's visual field center. On the contrary, rods dominate the outer parts of the retina and contribute allow for low-light vision. As one travels from the fovea into the periphery, the number of cones drastically decreases, while the number of rods increases. The photoreceptors contain photopigment proteins that convert light energy into chemical and electrical signals. Since object recognition relies on high acuity, the retinal image of the dog will be largely located on the cone-containing fovea. While the photoreceptors allow for the conversion of visual information into electrochemical signals, the structures immediately after play a crucial role in preliminary contrast processing that allows for more complex processing in the brain.

The diverse connections within the intermediate retina create an interwoven network consisting of excitatory and inhibitory inputs leading to contrast enhancement. In the case of the dog, the enhancement of contrast will allow a viewer to discern the dog from the background, and distinguish other finer details such as the eyes from the rest of the face. While the initial modulation begins subsequently in the bipolar cells with the aid of lateral communication of the horizontal cells, the bipolar cells also act as interneurons to communicate the signals from the photoreceptors to the innermost part of the retina containing the retinal ganglion cells (RGC).

While these cells were originally thought to largely only play the role of transmitting signals to the brain, recent research revealed that the diverse nature of these cells play an important role in early visual processing enabling more complex processing in later visual structures and areas (Brackbill et al., 2020). Researchers have discovered about 20 types of RGCs through molecular and functional classification (Brackbill et al., 2020; Kim et al., 2021). While each type has a unique functional characteristic, all share the concentric-circle receptive field organization similar to that of the bipolar cells. Briefly, a receptive field is a region of space, in this case, visual space, where a neuron's activity can be modulated by the presentation of stimuli. The entire visual field is tiled by receptive fields at each level of the visual system (*i.e.* retina, thalamus, cortex).

As mentioned before, bipolar cell's communication with the RGCs with the addition of lateral connections via horizontal cells leads to the emergence of light contrast detection. These "edge detector" cells contain receptive fields with both an excitatory and inhibitory region. The activity of the cell is directly related to the proportion of each region that is illuminated. In the case of the dog, the RGCs will aid in processing related to discriminating edges of the dog relative to the background or if the dog is moving (Figure 1.2). As mentioned earlier, the RGCs also play the role of sending signals to the brain via the optic nerve, the bundle of RGC axons.

Figure 1.2: Contrast processing of a dog at the level of the retina.

1.1.2 Lateral geniculate nucleus of the thalamus

While the first step of additional processing is in the lateral geniculate nucleus (LGN) of the thalamus, the inputs from the retina only make up a small proportion of the total inputs to this area (Usrey and Alitto, 2015; Van Horn et al., 2000). These inputs initiate activity while the feedback projections from the visual cortex and other brain structures modulate activity in early visual processing; however, these processes are not well understood (Usrey and Alitto, 2015).

1.1.3 Primary visual cortex (V1)

Contrary to the LGN, whose inputs are largely feedback from higher visual cortex, primary visual cortex (V1), within the occipital lobe, receives the majority of its projections from the LGN. In a manner similar to the retina, several LGN neurons synapse onto the same V1 neuron and condense signal information. Just as the photoreceptors and horizontal cells caused a concentric receptive field structure that is also shared by RGCs, the convergence of several LGN cells onto a V1 neuron leads to new receptive field structures, which can explain some of the new selectivity characteristics that arise in primary visual cortex.

The convergence of several LGN neurons with overlapping receptive fields onto a single V1 neuron results in two different neuron types: simple and complex. Simple cells have well-defined, elongated, and elliptical-shaped receptive fields consisting of adjacent excitatory and inhibitory regions (DeAngelis et al., 1995; Hubel and Wiesel, 1959, 1962). In line with the hierarchical theory, where lower-level cells feed into higher-level cells, researchers believe that the summation of LGN inputs leads to receptive field shape and function (Hubel and Wiesel, 1962). As mentioned earlier, LGN cells have concentric circle receptive fields that when aligned by excitatory regions and slightly overlapped resemble the receptive field shape seen in studies of V1 simple cells. Experiments using geometric stimuli, such as bars and edges, to measure the responses of isolated single neurons revealed selectivity to a small set of stimulus characteristics in simple cells (Hubel and Wiesel, 1962). Specifically, simple cells are optimally activated when a stimulus matches their orientation, size, and direction preference while lying within or traversing the excitatory region of the receptive field. Many studies have found, despite the sample, a diverse representation of preferred orientation and size (Hubel and Wiesel, 1959, 1962; Movshon et al., 1978b). Additionally, simple cells compute linear summation of responses to stimuli within the receptive field and are equal to the summed responses to individual stimuli (Movshon et al., 1978b). However, there is a population of simple cell neurons that have non-linear summation patterns, where the sum of the individual responses were less than the response to all the stimuli at once. Currently, researchers hypothesize that the two types of summation allow the cells to process information about the spatial arrangement of stimuli, which is increasingly important in complex visual scenes that exist in the natural world. Due to the nature of the specific selectivity present in simple cells, it is thought that they place a crucial role in the ventral stream processing, also referred to as the object recognition pathway.

In line with the name, complex V1 neurons have more complicated receptive field structures and less defined stimulus preferences. The receptive field consists of a diffuse region that is responsive to both light and dark stimuli (DeAngelis et al., 1995). While complex cells demonstrate orientation preference when exposed to orientation-varied stimuli, similar to simple cells, they do not share the other stimulus preferences. For example, simple cells will respond strongly to stimuli that match their particular orientation, size, and direction preferences, while complex cells respond strongly regardless of the position of the stimulus within the receptive field as long as it aligns with its orientation preference (Hubel and Wiesel, 1962; Movshon et al., 1978a). Due to the nature of the diffuse and less selective response properties, simple cells are thought to provide feedforward inputs to complex cells (Alonso and Martinez, 1998; Hubel and Wiesel, 1962). Also, unlike simple cells, all complex cells perform non-linear summations of stimuli within the receptive fields, which are thought to be important for the extraction of complex information from the visual environment by enhancing the desired stimulus and suppressing the non-preferred stimuli (Movshon et al., 1978a). Additionally, the characteristics suggest that these cells are important for processing related to visual motion and spatial arrangement of stimuli within the environment and may play a crucial role in the dorsal stream, which is responsible for guiding motions and the location of objects in the visual field.

Using the example of a dog, simple cells would likely respond to the edges and contours that match the preference of the cell and that make up the outline of the dog, such as details of the body and limbs (Figure 1.3). In contrast, the complex cells would respond to the overall shape and direction of movement of the dog rather than the low-level features. Even though these two cell types cover a diverse range of selectivity and processing, at this processing level higher-level features of the dog such as texture, color, depth, and form are still out of reach of the viewer. Recent research has focused on studying the processing in V2 in order to elucidate the transformations of information relating to object recognition from V1 to V2 (Figure 1.1).

Figure 1.3: Edge processing of a dog at the level of primary visual cortex. The additions on top of the dog's edge represent the receptive fields of simple cells in primary visual cortex.

1.1.4 Visual area V2

While some simple cells act as feedforward inputs to complex cells to generate different receptive field properties, others act as direct inputs to V2 (El-Shamayleh et al., 2013). The convergence of simple and complex cells onto a V2 neuron gives rise to a diverse set of selectivity properties that represent features common in the visual world. Seemingly similar to complex cells, V2 neuron receptive fields possess a large diffuse region void of obvious excitatory and inhibitory regions. Since the processing performed by complex cells closely aligns with that of the dorsal stream, one may hypothesize that the primary drivers of ventral stream V2 are simple cells (Hegdé and Van Essen, 2000). To bridge the understanding of the processing that occurs between V1 and V2, recent studies have searched for the presence of texture selectivity, as a function of naturalness, in both areas (Freeman et al., 2013; Ziemba et al., 2019). Representing natural characteristics in texture relies upon matching the statistical elements, such as image correlations and overall luminance so that there are no biases leading to differing responses between the two texture types (Portilla and Simoncelli, 2000; Victor and Conte, 2012). Using carefully constructed textures, V2 neurons demonstrate the emergence of naturalistic texture selectivity (Ziemba et al., 2019). Additionally, few V1 neurons display texture selectivity at longer latencies than seen in V2, suggesting that this selectivity arises due to a feedback mechanism. Currently, several labs are conducting physiological experiments to reveal the intricacies of texture selectivity in the visual cortex. A simple example of the processing found at this level of the visual system is represented in Figure 1.4

Figure 1.4: Texture processing of a dog at the level of area V2. The circle highlights what may be considered a natural texture, in this case, the fur of a dog.

While researchers currently explore texture in V2, selectivity for other higher-level features within the visual world, such as contours and simple shapes, have been superficially explored in V2. Research utilizing a diverse stimulus set containing numerous subclasses identified by their key characteristic (simple bars, intersections, acute angles, complex arcs, etc.) revealed a preferential response to stimuli belonging to a single stimulus type (Hegdé and Van Essen, 2000). Most notably, the recorded neurons have increased responsiveness to stimuli containing acute curvatures, which is thought to be important for the processing of closed contours. These findings suggest that elementary shape processing begins in V2; however, the extent of the contour and simple shape preference is unclear.

1.1.5 Visual area V4

In contrast to V2, shape selectivity has been extensively studied in visual area V4 through the presentation of simple angles, curves, and simple shapes (Pasupathy and Connor, 1999, 2001). As a preliminary experiment, V4 neurons responded preferentially to some curve stimuli, while being unresponsive to others (Pasupathy and Connor, 1999). Notably, the preferred responses followed a unimodal tuning for a subset of stimuli presented at a particular orientation as well as relatively matched in the degree of curvature. Building on top of the curve tuning, the presentation of shape stimuli, constructed to have either 2, 3, or 4 convex projections (Figure 2.7), revealed response modulation to boundary segments of a stimulus rather than the entire shape (Pasupathy and Connor, 2002, 2001). Additionally, as mentioned in previous visual areas, V4 neurons are sensitive to the location of the shape feature relative to the center of the receptive field. In order to successfully capture the neural responses to the shape set, Pasupathy and Connor 2001 devised a model composed of the product of several Gaussians (see methods: APC model for more details). While the original model includes 4 Gaussians, further analysis suggests that only 2 are necessary to predict responses to stimuli regardless of the position within the receptive field. Specifically, curvature and angular position are the primary drivers of the response and are sufficient to capture the majority of the shape tuning. As mentioned earlier, this suggests that V4 is selective for contours defined by particular curvature and angular positions rather than entire shapes or objects. Researchers corroborate this finding in other studies using dynamic and evolutionary stimulus construction to determine the optimal stimulus (Carlson et al., 2011).

Further, the position-invariant selectivity for a small segment of the shape boundary gives insight into how V4 represents shape within a neural population. Using the APC model and the data exhibiting shape tuning, researchers simulated neurons that spanned the curvature and angular position space. These new synthetic neural populations allowed Pasupathy and Connor (2002) to reconstruct the original stimuli used in the experiment. The success of this effort argues that a diverse neural population within V4 may use population coding as a plausible method of encoding shape. However, the population construction assumes stimulus presentation occurs within a neurons' perfectly overlapping receptive field boundaries. While these characteristics are not representative of a real population's receptive field organization or of object arrangement in the visual world, the model still provides important insight into shape selectivity and how neural activity may encode shape within the brain. However, we require further research and technological advancements that allow for large-scale and high-resolution recordings before we can test whether population coding is present in a recorded V4 population. This is represented by Figure 1.5.

Figure 1.5: Shape processing of a dog at the level of area V4. The shapes give a simplified representation of the processing happening at this stage in the visual hierarchy.

Since V4 neurons are selective for curvature, researchers questioned whether V4 will show similar selectivity for scaled stimulus features. When we scale a stimulus, the absolute curvature will change, while the normalized curvature will remain the same. This is because absolute curvature decreases as the size increases due to the angular sampling width. On the other hand, scaling the angular position window accordingly, will not affect the normalized curvature. In order to determine whether V4 codes for a size-invariant representation of shape, crucial for a robust object recognition pathway, researchers determined the optimal stimulus for an isolated neuron and presented it at several scales within the receptive field (El-Shamayleh and Pasupathy, 2016). From the following analysis, the majority of the neurons' responses did not shift in curvature preference, representing a selectivity for normalized curvature. However, a smaller proportion exhibited a shift in curvature preference, representing selectivity for absolute curvature features. Since both types of selectivity are present, they likely play separate roles: normalized curvature preference for size-invariant object recognition and absolute curvature for information related to interacting with one's environment. Additionally, the size-invariant representation of shape brings us closer to understanding object recognition. However, we are unable to accurately mimic the responses of neural populations since current research places stimuli within a single-unit's well-isolated receptive field and not across many receptive fields that tile visual space.

While the APC model proposed by Pasupathy and Connor (2001) revealed many intricacies of shape representation and described the responses in V4, other studies propose models that aim to understand the derivation of shape selectivity from lower-order inputs. Researchers constructed a model from several neural layers, representing selectivity and invariance operations in V1, V2, and V4 (Cadieu et al., 2007). The model is a subset of neural layers isolated from an object recognition model aimed at understanding the mechanisms and transformations that lead to robust object recognition. (Cadieu et al., 2007; Serre et al., 2007). The V4 model utilizes hierarchical theory so that simple and complex cells feed into V2 which then project to V4. Additionally, it has been successful in replicating the results from the APC model (Cadieu et al., 2007; Pasupathy and Connor, 2001). The model success suggests that the edge detector simple cells play a crucial role in form processing while the complex cells are important for creating translation-invariant responses for stimuli within the receptive fields (Cadieu et al., 2007). Additionally, the convergence of these units onto V2 neurons acts as an explanation of early selectivity for contours and corners while also including characteristics like position-invariance that has been previously found in V2 (Hegdé and Van Essen, 2000).

1.1.6 Visual Area IT

While V4 is currently known to be selective for a segment of a shape boundary within a receptive field, neurons in the inferotemporal cortex (IT) show preferential responses to entire complex shapes and objects that exist within our visual world (DiCarlo et al., 2012; Fujita, 2002). Due to the convergence of afferents from lower-level visual cortex to a single IT neuron, the resulting receptive field consists of a diffuse region that is larger than those in lower-level visual cortex (Fujita, 2002; Gross et al., 1969). Additionally, many of the cells share a bilateral representation of the world, meaning that there is no longer the presence of a retinotopic mapping since all cells respond to input from both eyes (Rodman et al., 1993). However, some rough topographic organization is present in the posterior regions of IT, but quickly deteriorates when moving into more rostral areas. This suggests that a new organization pattern may be present in the form of object or task-dependent groupings (DiCarlo et al., 2012). As one may expect from some characteristics of earlier visual cortex, the receptive field properties of IT neurons lead to a variable tolerance to transformations in position, rotation, and scale across a population of neurons. While some single units demonstrate minimally varied responses to preferred stimuli with presentation changes, others demonstrate narrow tuning properties with much larger diminished responses as a stimulus undergoes a transformation (Fujita, 2002). Due to the diversity existing within a population, researchers began to hypothesize the role of a single IT neuron in object recognition.

Jerome Levittin presented the observation of the existence of specialized cells, known as “grandmother cells”, that are responsible for the recognition of particular objects (Gross, 2002). In essence, he hypothesized that there was a neuron that would respond when a subject saw a specific object or person, like one's grandmother. While the hypothetical neuron gained traction and led to exploratory experiments, many were hesitant to adopt the idea. Some major concerns related to the limitation of a finite number of neurons representing an infinite number of objects. Due to this limitation, others suggested that a population code would be more appropriate in capturing the infinite number of possibilities of objects, familiar and unfamiliar, within the visual world. Pasupathy and Connor (2002) exemplify population encoding in V4, and therefore IT neurons may also interact to create a population code to achieve robust object recognition. However, while it is understood how a single V4 neuron may contribute to the population response, it is not currently understood how a single IT neuron contributes and plays a role in object recognition (DiCarlo et al., 2012; Pasupathy and Connor, 2002, 2001). Fortunately, recent research has dived into exploring whether "grandmother cells" and how a single neuron may play a role in a population representation of objects.

To determine whether "grandmother cells" exist and how a single IT unit contributes to robust object recognition, some studies isolated single neurons with highly specific tuning properties and present the preferred stimuli with position shifts, rotation, and scale changes (Zoccolan et al., 2007). These specifically-tuned neurons mostly demonstrated minimal invariance to object transformations and therefore combat the hypothesis of the presence of "grandmother cells". One would expect that neurons that respond solely to a particular object would be robust to changes in position, scale, and viewing angle, however, the opposite seems to be true (Gross, 2002; Zoccolan et al., 2007). This finding suggests that there is population coding of objects in the visual system relying upon the diverse selectivity properties of many neurons. However, this does not directly inform us about how the robustness of the pathway arises.

Arguably, the most fascinating component of biological object recognition is robust categorization despite differences in activation as early as the retina. In the case of the dog, an upright dog and a rotated, scaled dog produce vastly different light patterns on the retina. Even though the initial activation differs immensely between the two conditions, the brain is able to categorize the object as being a dog and able further differentiate between various dog types. While this is not well understood, recent research extracted object identity from the responses from IT neurons, but not those belonging to earlier areas, corroborating previous work that object recognition capabilities arise in IT (Majaj et al., 2015). To establish a connection and understanding between human and nonhuman primate object recognition, Majaj et al. (2015) determined performance in an object recognition task for each model system. When comparing simulated V1, recorded V4, and recorded IT responses, they determined that IT populations were the first to allow for decodable performances similar to that of humans. This implies that object identity is a unique characteristic of IT, but does not give a mechanism of how it may arise in higher-level visual cortex and not earlier.

Using an approach consisting of mathematical modeling of neural data across several visual areas, researchers proposed a potential computational mechanism of how object recognition emerges and agrees with the findings from Majaj et al. (2015). Since biological object recognition systems are able to classify objects into categories and discriminate between objects regardless of environmental context, translations, and transformations while existing in a high-dimensional space, modeling is appropriate to understand the underlying characteristics of the information contained within the data. To explain some of the computations that may take place, we will walk through a hypothetical example. Imagine we plot the responses of 3 neurons to various presentations of a dog in a 3-dimensional space, where each dimension corresponds to a neuron. There should be a continuous surface, referred to as a manifold, that can be fit to the data across those three dimensions. In this case, we can imagine the presence of two manifolds: the “dog” manifold and the “non-dog” manifold. In the retina and lower-level visual areas like V1, the two manifolds are highly tangled representing an inability to discriminate whether the object is “dog” or “non-dog” (DiCarlo and Cox, 2007; DiCarlo et al., 2012). However, processing in later visual areas untangles the manifolds and allows for hyperplane separation (DiCarlo and Cox, 2007). As the information progresses through the visual pathway, the manifolds become less tangled and when reaching IT the manifolds exist in the least tangled state. If the manifolds are separable as mentioned earlier, then the biological system can categorize the object into either a "dog" or "non-dog". On the other hand, if the two manifolds share some coordinates, it still remains tangled and the decision about categorization is much more difficult.

While manifolds have proved useful in uncovering potential computations related to object recognition, other researchers have focused on building biologically plausible neural network models to understand and explain the processing occurring at each step of the visual system leading to robust object recognition. Introduced earlier in terms of providing a mechanistic model for visual area V4, Cadieu et al. (2007) provide an interpretation of the first several layers of a larger model of object recognition (Serre et al., 2007). As a review, the model incorporates current knowledge about the anatomy and physiology of the visual ventral stream into several neural layers. Importantly, this model acts as a feedforward explanation of how complex object categorization arises in the brain starting from simple V1 cells and ending in Anterior IT. Serre et al. (2007) trained the model on an image set with the goal of making the model characterize each image as either an animal or non-animal. The images contained a central object which varied in position in space, rotation and scale while also having various levels of background clutter. In order to compare the model to the human ventral pathway, they also conducted a human psychophysics experiment. The model demonstrated human-level performance to objects presented in minimally crowded environments regardless of the position, rotation, or scale. However, the model performance decreased as the amount of visual clutter increased, while human performance remained similar. The ability of the feedforward model to capture the majority of the invariance present within biological visual pathways proposes that the majority of the features present in IT are due to feedforward connections and processing. However, the inverse relationship between performance and the amount of clutter indicates a difference in the model construction and visual pathway anatomy and physiology. Largely, the lack of feedback connections negatively affects performance in crowded environments. The ability to enhance and discriminate objects from the background increases with the addition of these connections (Kafaligonul et al., 2015; Serre et al., 2007). While there is a large amount of research on how processing and characteristics of IT may lead to robust visual recognition, further research is necessary to understand how the biologically important process emerges.

1.1.7 Conclusion

In conclusion, while the ventral visual system has been extensively studied since the mid-twentieth century, more experiments are necessary to unveil both the processing within each visual area and how the processing relates to the robustness of the biological object recognition pathway. Continuing with the example of a dog in our visual environment, first, the dog casts an image onto our retina, consisting of light and dark patches, and leads to RGC activation and inhibition, respectively. The optic nerve transmits the signals to the LGN which are then sent to the primary visual cortex, V1, where selectivity for bars of various lengths, widths, and orientations arises. This selectivity allows for neurons to preferentially respond to the edges of the dog and its features that lie within their receptive fields. Additionally, there are complex cells that are responsive to the overall form and direction of the dog, which may be more applicable to the processing of the dorsal pathway. However, continuing in processing related to the ventral stream, V2 neurons may respond to the texture of the dog's fur as well as some simple shapes representing some of the dog's features. Next, the signals pass to visual area V4 which will process information related to complex shapes that make up the dog. Finally, the inputs into IT allow for object categorization and recognition so that our brain can interpret that the object we see is a dog as opposed to a non-dog (Figure 1.6; Figure 1.7; Figure 1.8).

Largely, we understand normal visual function, as detailed above, from analysis of adult neural recordings, however, some of these visual functions are not fully present at birth and instead strengthen and change over a developmental window. Current research aims to understand developmental changes for many important visual structures and areas for greater insight into amblyopia, a developmental visual condition, and the implementation of proper preventative and rehabilitative measures.

Figure 1.6: Object recognition capabilities in visual area IT. Using the information from previous visual areas, the brain is able to categorize the dog as a dog in the environment.

Figure 1.7: Object recognition capabilities robust to changes in scale and orientation. Even though this dog is a different orientation and scale, as well as placed in an irregular location within its environment, the brain is still able to recognize it as a dog.

Figure 1.8: Object recognition capabilities robust to changes within an object category. The presentation of a different dog in our environment is still recognizable by the brain as a dog. This begins to hint at the expansive biological object recognition pathway that has evolved within the brain.

1.2 Amblyopia: causes, treatments, and implications

Early in the 6th century, Hippocrates, a Greek physician and father of modern medical practices, noticed that some individuals with healthy-looking eyes displayed decreased acuity in one eye (Loudon and Simonsz, 2005). Due to the unknown cause of the condition, he and others prescribed fresh vegetables and other naturally occurring substances thought to improve visual function. The condition, traced to cortical deficits, became known as amblyopia which is Greek for dimmed or dulled vision (Figure 1.9). Currently, amblyopia prevalence estimates lie around 4% of the total world population (Kiorpes, 2019; Loudon and Simonsz, 2005). However, due to the sampling techniques and geographical/contextual locations used by various studies, published estimates range between 0.5-5.3% of the population (Loudon and Simonsz, 2005).

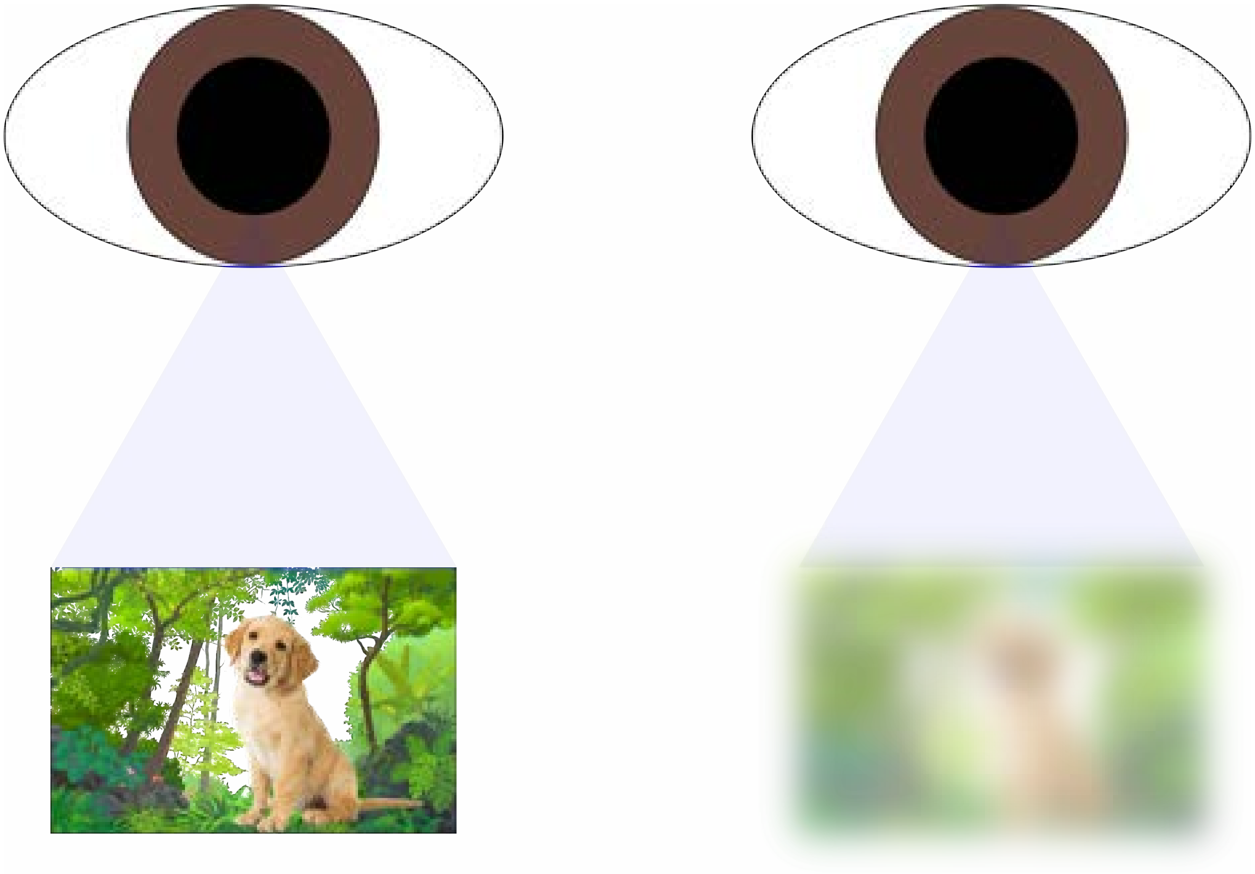

Figure 1.9: Visual representation of amblyopia. This condition is often referred to as ”cortical blindness” and leads to acuity differences between the eyes, despite both being healthy.

Even though the condition’s commonness is not precisely known, clinicians established that early treatment can be exceptionally effective at preventing and improving visual function. Paired with the understanding of the sensitivity of the visual system during childhood to abnormal visual input, researchers consider amblyopia a developmental visual disorder. The most common risk factors for children are asymmetrical refractive powers between the eyes (anisometropia), misalignment of the eyes (strabismus), and visual deprivation (Loudon and Simonsz, 2005).

The first and most common factor, anisometropia, causes difficulty focusing both eyes simultaneously due to the consensual nature of the accommodation reflex (Motlagh and Geetha, 2022). Importantly, the reflex varies pupil constriction, coordinates the muscles to direct the eyes to the same target in visual space, and contracts the muscles that control the thickness of the lens and focus an image onto the retina. For this particular risk factor, the contraction of the muscles around the lens is most impacted. Therefore, in order to compensate and obtain a clear image, the brain determines a dominant and preferred eye and uses it to obtain an in-focus image, while simultaneously suppressing visual input from the non-preferred eye.

Similarly, strabismus leads to suppression of input from the misaligned eye. This condition is commonly referred to as "lazy eye" and can cause serious visual impairment if not treated soon after the condition is observed. There are four main types of strabismus: inward turning (esotropia), outward turning (exotropia), upward turning (hypertropia), and downward turning (hypotropia) (Clarke, 1999). These misalignments are commonly noticed early in childhood, with an average diagnosis age of 7.4 years, and are less likely to develop in adolescence and adulthood (Attebo et al., 1998). Even though these variations differ in the direction of misalignment of the eye, the overall effect is the same as each other as well as in anisometropia: inability to focus both eyes properly. However, in this case, the issue lies in the ability of the eyes to focus an image onto both foveas, and therefore the muscles controlling the direction of the eyes are the most important.

Visual deprivation, the last risk factor, relates to total loss of acuity in a single eye to a point where visual function in that eye is unable to make a significant improvement (Voss, 2013). However, while this may seem to only reference total blindness, it also includes both conditions mentioned above (Morishita and Hensch, 2008). The singular use of the preferred eye will cause a deprivation of the other eye as the brain will learn to "ignore" the inputs.

Currently, there are two primary treatments for those with amblyopia as long as there is some functionality of the amblyopic eye, therefore excluding those with total visual deprivation. The overall goal of the treatments is to increase the use of the amblyopic eye. So for those experiencing refractive differences between their eyes, it is common to correct the differences using prescription eyeglasses to place a clear image onto the retina of both eyes (Holmes and Clarke, 2006; Webber and Wood, 2005). For those with a misalignment of the eyes, either a patching method or the introduction of a pharmaceutical to the healthy and preferred eye will lead to a decrease in the visual input in the healthy eye and force a greater reliance upon the amblyopic eye. If the strabismus does not improve or disappear, surgical intervention is necessary to prevent further visual deficits (Webber and Wood, 2005). These treatments are most effective immediately upon diagnosis/discovery of the conditions.

Unfortunately, some public-health advisors have declared that treatment for amblyopia is unnecessary as there was no apparent evidence of disability (Holmes and Clarke, 2006). However, recent clinical research in humans found that decreased visual acuity in a single eye can have an adverse effect on disability and perceived disability, psychosocial development, and coordination of visual information and motor output (van de Graaf et al., 2010; Webber and Wood, 2005).

Researchers estimate that half of the people with paid positions and amblyopia have difficulty completing their job (Rahi et al., 2002). While some are able to continue working, many others are forced to resign or are terminated from their position. This translates over to other life difficulties with an increased risk of injury and death related to impaired visual function. While amblyopia can be an invisible condition, those with obvious strabismus are unable to conceal their condition causing further difficulties in obtaining employment. Overall, while there is notable self-reported disability, there are cases where overly perceived disability can lead to a lower quality of life for those affected by amblyopia.

While decreased visual acuity is a primary concern for those with amblyopia, many amblyopic patients experience reduced binocular vision (stereopsis). Typically, these deficits are most common in those who experience risk factors around 3-18 months of age without treatment (Fawcett et al., 2005). However, the development of a risk factor, most commonly strabismus, during the first several years of life can also increase the chance of decreased stereopsis. These can contribute to the deficits in certainty in spatial location, motor output, and balance, and in tasks that require a 3d representation of cues (Webber and Wood, 2005). Most importantly, decreased depth perception can affect fine motor movements which may also be crucial to learning during early education and development.

Both amblyopia and the presence of strabismus has led to additional psychosocial issues in children, teenagers, and adults. Research studies reveal that many teenagers and adults with these conditions exhibit decreased self-esteem, increased embarrassment, and diminished ability to meet and interact with new people (Eustis and Smith, 1987; Nelson et al., 2008; Satterfield et al., 1993). Additionally, parents report that young children with esotropia can cause a declined parent-child relationship due to decreased eye contact (Eustis and Smith, 1987). While the parents are giving a third-person account of the effect of the condition on a child, the reports are highly correlated with the self-reports of those with amblyopia. Early treatment of amblyopia and addressing of psychosocial issues can be crucial for a child's ability later in life to form meaningful relationships. If not treated early, the psychosocial deficits can worsen throughout teenage and adult years leading to further difficulty (Nelson et al., 2008; Webber and Wood, 2005). Luckily, corrective surgery of the misaligned eye so that the amblyopic deficits are not as noticeable remedies many of the psychosocial issues related to strabismus. Further research into effective treatment and preventative strategies can minimize the adverse effects of the condition that many face.

While amblyopia still affects a relatively large percentage of the population, the treatments reviewed above have drastically improved the condition for many individuals. Researchers developed and implemented treatments by conducting research that focused on understanding the visual system and how it develops. In order to effectively understand how researchers constructed research questions and how they were able to give insight into the physiology of the developing visual system, we will briefly review the development of the visual system and its functions.

1.3 Development of the visual system

As mentioned previously, clinicians created effective treatments of amblyopia built upon research on the neural basis of visual development to uncover the mechanisms associated with normal and abnormal visual experiences. At birth, humans are estimated to be born with poor vision, which then develops rapidly over the first several months to years of development (Figure 1.10). Since research studies on humans are quite limited to either behavioral or functional imaging techniques, researchers have used model organisms, like the cat and the monkey, to understand developmental changes in characteristics present in either single neurons or populations of neurons. Importantly, these studies allowed for an increased understanding of visual development and extrapolation to human development.

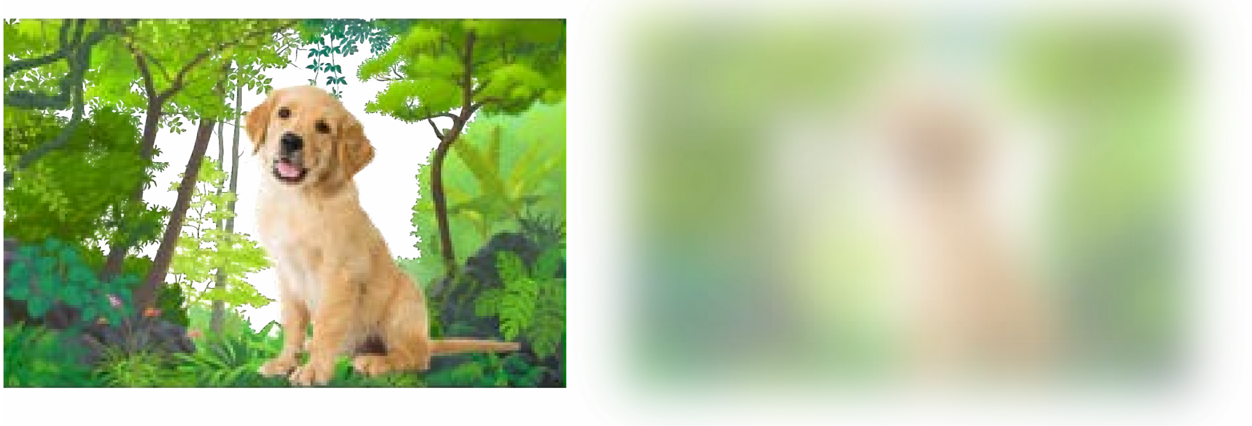

Figure 1.10: Adult and infant vision. Adults typically have high acuity and well-functioning visual functions (left), however, infants are born with poor visual function as demonstrated on the right.

However, in order to appropriately generalize the findings in these model organisms, some important considerations are necessary. When choosing a model organism the researchers must understand what limitations each model organism poses, and then choose the organism that can be effectively used to study their question. Within the last 50 years, non-human primates have become an important model system due to the similarities between monkey and human visual cortex (Boothe et al., 1985; Kiorpes, 2016). As hinted in the visual system overview, these organisms share a large amount of the structure, functional, and developmental characteristics with humans. However, there are many powerful model organisms that share limited similarities with humans. Mice, for example, have visual characteristics that differ from humans in terms of acuity and binocular vision but are powerful tools for understanding the circuitry and molecular and genetic mechanisms that play a role in visual processing and development (Kiorpes, 2016). These subfields of visual neuroscience are currently inaccessible in a primate model, but may become more common within the coming decades.

Due to the nature of developmental research questions and the necessity of finding translatable potential treatments for humans, cats, and monkeys are common model organisms for these experimental questions. Importantly, the use of these organisms shifted the understanding of visual development immensely within the last several decades and allowed for exciting approaches to further understand development so that human visual disorders can be effectively treated.

Before researchers used empirical approaches to explore the level of visual function present at birth, the consensus was that human infants were born blind and that all visual functions reached maturity over the course of years (Kiorpes, 2016). Additionally, researchers thought that as time passed, human vision became less vulnerable to various visual experiences. In line with this hypothesis, Wiesel and Hubel found experimental evidence of critical periods, short periods of neural sensitivity to experience, in cat LGN and V1 (Wiesel and Hubel, 1963a, 1963b). In order to effectively study the effect of visual deprivation, the researchers monocularly deprived several cats of visual input by suturing the eyelid or introducing a translucent eye cover at different periods after birth. The two most extreme groups contained cats deprived of normal visual experience at birth and those deprived late into adulthood (Wiesel and Hubel, 1963b). The control cats, with no visual deprivation, showed an ocular dominance distribution with most neurons responding to inputs to either eye following a normal distribution where a smaller set of neurons are either responsive to the right or left eyes. The aggregation of data across many cats and electrode penetrations allowed the comparison of experimental measures of eye-preference distributions to an expected distribution. In agreement with the hypothesis of short sensitive periods of plasticity, the young cats visually-deprived in one eye showed a distribution of neurons that predominately responded to inputs to the normal eye. In other words, the deprivation of a normal visual experience caused a shift in the organization of V1, and neurons originally dedicated to the deprived eye became responsive to input from the normal eye. In contrast, when researchers introduced adult cats to abnormal visual experiences for several months, the organization of the ocular dominance of neurons remained unchanged, representing the ocular dominance distribution of cats in the control condition. These findings support the concept of increased sensitivity periods to visual experience early in an organism's visual development. However, neural plasticity allowing for visual reorganization fades over time as demonstrated by the unaltered distribution of ocular dominance after visual deprivation of adult cats. The experimental evidence supporting the concept of short, increased-plasticity periods based on visual experience spurred research to explore the response characteristics of neurons along the visual pathway, the capabilities of various visual functions with behavioral paradigms, and the critical periods of visual functions.

Since the hypothesis of critical periods before Hubel and Wiesel dictated that visual functions likely develop on the same time scale, researchers started looking for the existence of bottleneck neurons that could act as a rate-limiting step of development within the early visual system (Kiorpes, 2016, 2015). The presence of such neurons within the early visual pathway, like the retina or LGN, could act as a simple supporting explanation of the hypothesis of synchronized visual function development where all visual functions reach adult levels of sensitivity at similar times. However, the comparison of true infant performance and an optimal system suggests the retina does not have the ability to act as the developmental limiter despite the maturation characteristics present within the first several months of development (Kiorpes, 2016; Springer and Hendrickson, 2005). Similarly, other studies focused on the LGN to uncover some potential developmental effects, but found that the LGN did not act as a hindrance to visual development progression (Movshon et al., 2005).

Despite this, researchers discovered developmental changes in the LGN's temporal dynamics and visual functions. Initial research discovered that monocular deprivation of an eye led to atrophy of the neurons originally receiving inputs from the eye (Wiesel and Hubel, 1963a). However, despite the differences in size, there were no differences in the ability to discriminate between stimuli at small differences in spatial arrangement and therefore suggests the presence of adult-like spatial resolution at birth (Blakemore and Vital-Durand, 1986a; Movshon et al., 2005). Similarly, other studies found no considerable difference in the organization of the receptive field between infant and adult LGN neurons but differences in the responses to continuous stimulation, overall response magnitude, and latency (Blakemore and Vital-Durand, 1986b; Hawken et al., 1997; Movshon et al., 2005). Researchers pointed to the neural development of the visual cortex as the potential limiting factor of development (Movshon et al., 2005).

In order to build upon the research that kickstarted the research into development by providing experimental evidence for critical periods, Hubel and Wiesel (1963) studied young cats with no previous visual experience. The response characteristics in the striate cortex were similar to that seen in adult cats with clear demonstrations of orientation-selective simple and complex cells (Hubel and Wiesel, 1963). Additionally, kittens that were monocularly deprived from birth demonstrated response characteristics that were considered normal if observed in adults leading to the assumption that the connections that allow for the activity to these stimuli are present at birth or shortly after. Importantly, this suggested that monocular deprivation would have little effect on the functional properties. However, as mentioned earlier, the organizational properties of the primary visual cortex are heavily influenced by visual experience (Wiesel and Hubel, 1963b). Research conducted on monkeys found that the critical period for the organization of the striate cortex, binocular properties, and contrast sensitivity in monkeys spanned several weeks after birth (Blasdel et al., 1995; Chino et al., 1997; Zheng et al., 2007). Additionally, some temporal dynamics relating to transient responses and response magnitude matched that seen in adults, both in terms of reliability and latency, within the first several weeks of development (Zhang et al., 2008). Characteristics similar to those observed in V1 neuron development are found in V2 in terms of functional organization and temporal dynamics, among others (Maruko et al., 2008; Zhang et al., 2008; Zheng et al., 2007).

As seen in earlier visual structures and areas, visual area IT neurons in young monkeys demonstrate similar receptive field properties to that of adults in matched conditions (Rodman et al., 1993). Additionally, as found in studies of V1 and V2, the IT neuron response latencies were longer and response magnitudes were lesser than that of adult IT. Importantly, the research also focused on characterizing the neurons' functional properties and found that boundary curvature, faces, and other stimuli elicited responses similar to those recorded in adult cortex as early as 2 months of age. However, this IT-specific selectivity refined further with age and Rodman et al. (1993) estimated that selectivity to complex shapes and objects matured within about 6 months to show selectivity levels that parallel adult IT.

While previous sections have focused on the neural changes during development, there is also a wealth of literature that use behavioral paradigms to monitor the developmental changes to several higher-level visual functions (Harwerth et al., 1990; Kiorpes, 2016, 2019). This is a particularly important contribution to understanding visual development because it allows for a deeper understanding of visual characteristics that are measurable in humans with current technology; These include spatial contrast, global motion and form, pattern motion, and contour integration (Kiorpes, 2016). Additionally, these behavioral approaches allow for the understanding of unique critical periods for each visual function and have demonstrated a different temporal profile for the change of sensitivity over time.

As seen above, researchers have used both neurophysiological and behavioral approaches to study the development of LGN, V1, V2, and IT. Currently, researchers do not know much about the developmental time course of V4 response characteristics in either temporal or functional contexts due to the lack of such studies. Specifically, a deeper understanding of the neural correlates of higher-level visual functions like global form perception can play an important role in uncovering the mechanisms behind developmental conditions like amblyopia. Therefore, further research is necessary to elucidate some mechanisms behind some developmental conditions, like amblyopia, as well as understanding how robust object recognition capabilities arise within the brain.

1.4 Experimental design

In order to gain insight into how the neural basis of shape selectivity may evolve over a developmental period, we collected population responses to shape stimuli using 96-channel Utah arrays from the ventral visual areas in developing macaque monkeys. Using our stimuli set of 13 shapes with a primary parametrically varied curvature component, presented at several orientations, and the recorded neural responses we implemented two models. Constructing models of the visual system can prove to be useful for understanding processing that occurs as visual information passes through visual areas and be used/taken into consideration when devising rehabilitative techniques or technologies. For example, the development of a visual cortical prosthetic that mimics the capabilities of our ventral stream will be more successful if constructed with biologically-plausible techniques. The first model, the APC model, corresponds to previous work that found that modeled V4 responses by the angular position and curvature of a shape feature (Pasupathy and Connor, 2001). The second model, the ICL model, represents processing that is thought to be present early in the visual system on the level of the retina and allows us to track changes in V4 shape selectivity over time. We measured and compared the performance of these models across many different conditions to draw conclusions on development. Overall, this project has several hypotheses:

1. We will observe shape-modulated responses in visual area V4 and not other visual areas.
2. The APC model will be successful in explaining many sites in visual area V4, but not other areas.

3. The ICL model will be unable to explain sites in the ventral visual pathway, and therefore will act as a baseline for developmental comparison.
4. We will observe stable shape selectivity characteristics across developmental time points.

CHAPTER 2

METHODS

2.1 Data collection

The visual neuroscience laboratory (VNL) at New York University conducted experiments with four macaque monkeys (Macaca nemestrina) to study the activity of neurons in visual areas V1, V2, V4, and IT Figure 2.1. To record the multi-unit activity, VNL implanted two 96-channel multielectrode “Utah” arrays (Blackrock Microsystems) along the V1/V2 border and V4 in two of the monkeys, and one array in IT in the other two. VNL guided their placement decisions using gross anatomical features, while avoiding major blood vessels.

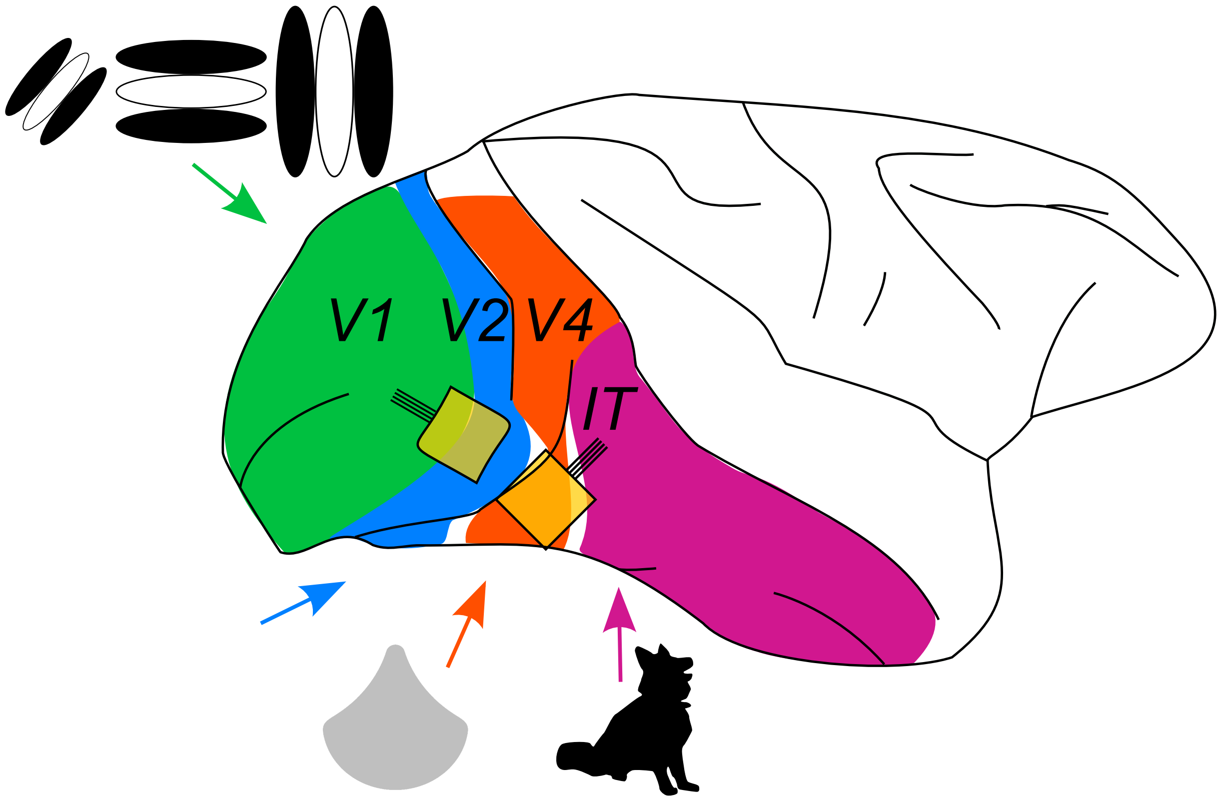

Figure 2.1: A schematic of the brain and ventral visual areas and their selectivity characteristics.

Throughout the first year of life, VNL made repeated measurements by recording simultaneous activity from the visual areas. VNL detected multi-unit spikes by comparing raw voltages to a threshold set 3.5 standard deviations above a pre-experimental baseline. For all analyses, the author uses units of spikes per second (spikes/sec) computed over a response window of 150 ms beginning with the estimated response onset and ending at the conclusion of the interstimulus period.

VNL trained the monkeys to passively fixate on a centrally located square, spanning 0.1 degrees of visual angle, while shape stimuli flashed around 1 degree parafoveally (Figure 2.2). To ensure that VNL placed the stimuli within the recorded neurons' receptive fields (RF), they used a flashing stimulus to map the RF location prior to stimulus presentation. Additionally, VNL used an infrared eye-tracking camera (EyeLink 1000, SR Research, ON) to confirm that the monkey's participation in the passive fixation task. In situations where the monkey broke fixation, the stimulus presentation pipeline reset the current stimuli sequence and we discarded the responses to isolate those that were stimulus-evoked.

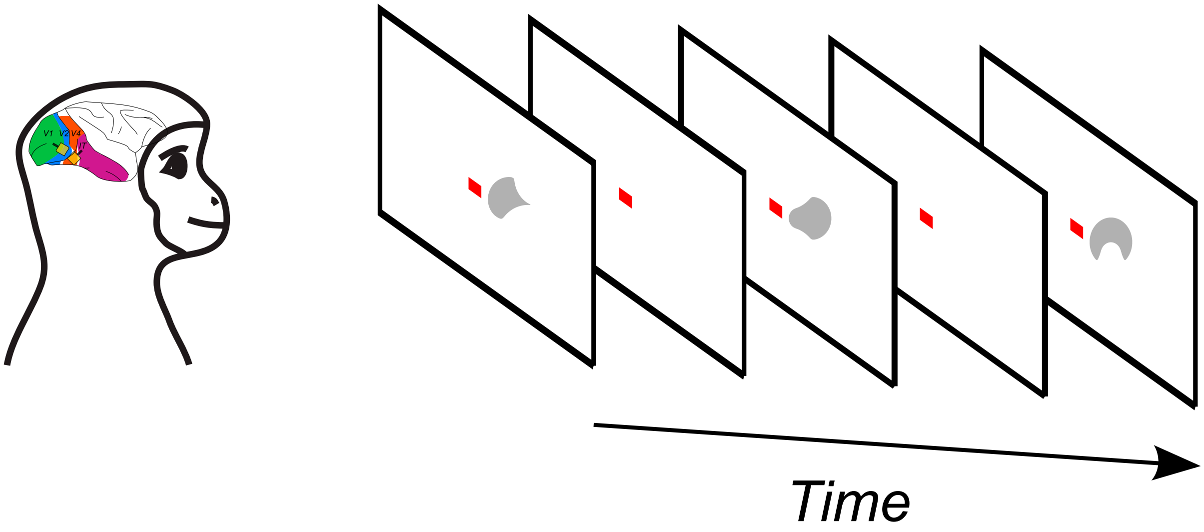

Figure 2.2: Data collection. The red square represents the fixation point.

2.1.1 Stimuli

VNL used the 13 shape stimuli set (Figure 2.3) from El-Shamayleh and Pasupathy (2016) consisting of 6 convex, 1 circle, and 6 concave stimuli so that we could tile a curvature space. Each stimulus had a primary parametrically-varied curvature component presented at either 4 (0° - 270°, at 90° steps) or 8 (0° - 315°, 45° steps) orientations. All stimuli were shown 2° of diameter in visual space, except for those in IT shown at 1°, and presented at the center of the population RF. During the experiment, VNL presented individual stimuli, within a group of 8, for 100 ms with a 100 ms interstimulus interval. To determine the spontaneous firing rate of the recorded multi-units, VNL randomly dispersed "blank" stimuli matched the screen color and luminance. The blank stimuli and interstimulus period are equivalent in appearance, but differ in placement within a stimulus presentation sequence: blanks are random and the interstimulus periods are systematic, respectively. Lab members presented each stimulus a minimum of 30 times, randomly dispersed throughout trials, in order to capture the response properties of the multi-unit sites. The lab collected data from one, several hour long, recording period for each monkey.

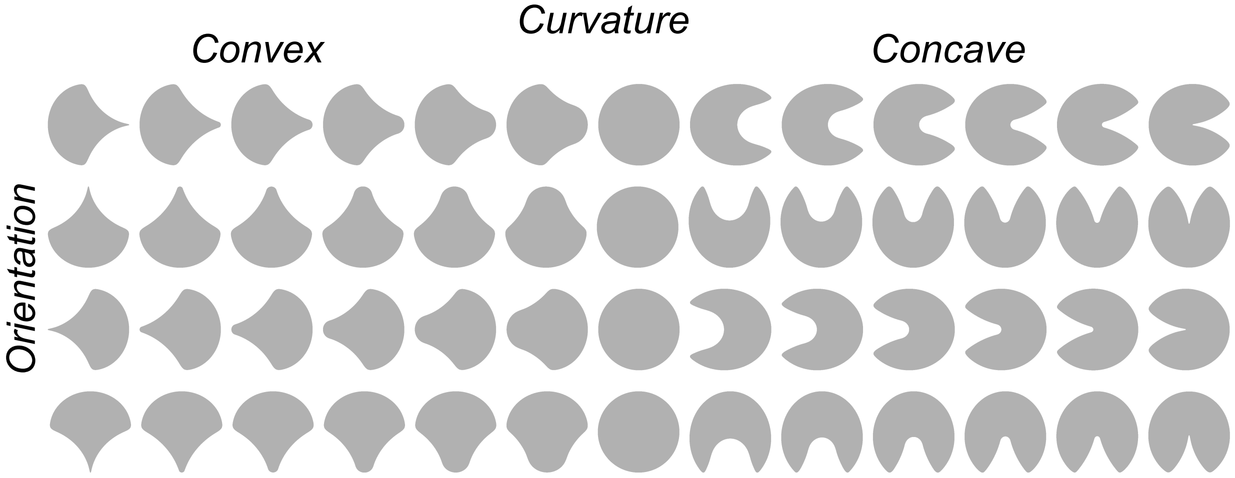

Figure 2.3: Stimulus set used in the multi-unit data collection. There are 13 unique shapes each shown at 4 orientations.

2.2 Analysis

2.2.1 Visually-responsive sites

To determine sites that exhibited visually-evoked activity, the author split and compared time-matched, repeated stimulus presentations through the use of split-half correlation. This analysis aims to distinguish sites that have meaningful responses from noisy ones. A greater value corresponds to a site that is less noisy and has a tuning element. The author determined a threshold value to discern sites producing predictable and non-random firing patterns. More specifically, to determine the threshold, the author sorted the sites by correlation coefficient and picked a value at which visual responsiveness disappeared. If there were sites with values below the threshold, the author discarded them since they represented noisy and unresponsive sites. The author isolated sites above the threshold for all analyses.

2.2.2 Angular position and curvature (APC) model

For analysis with the APC model, below, the author converted the stimuli into a set of 8 angular position and curvature coordinate pairs by computing the turning angle around 8 unequally spaced main feature curvature components. In order to have consistent and reproducible sampling, the author used the center of mass of each shape to determine the angular position of the main shape features. For all analyses, 0° and 180° correspond to the right and left directions, respectively (Figure 2.4). The author converted the turning angles into degrees of curvature ranging between -1 and 1 with a logistic function Equation 2.1. C_S is the transformed curvature. α represents the squashing strength, and C_r are the measured turning angles. The most concave stimulus had a primary feature with a curvature measurement segment of about -1, corresponding to a strong concavity and the strongest convexity had a value of about 1. A curvature feature with a curvature of 0 represents a flat segment, corresponding to a turning angle of 180° (El-Shamayleh and Pasupathy, 2016; Pasupathy and Connor, 2001).

$$C_s = \frac{2}{1 + e^{-\alpha C_r}} - 1 \tag{2.1}$$

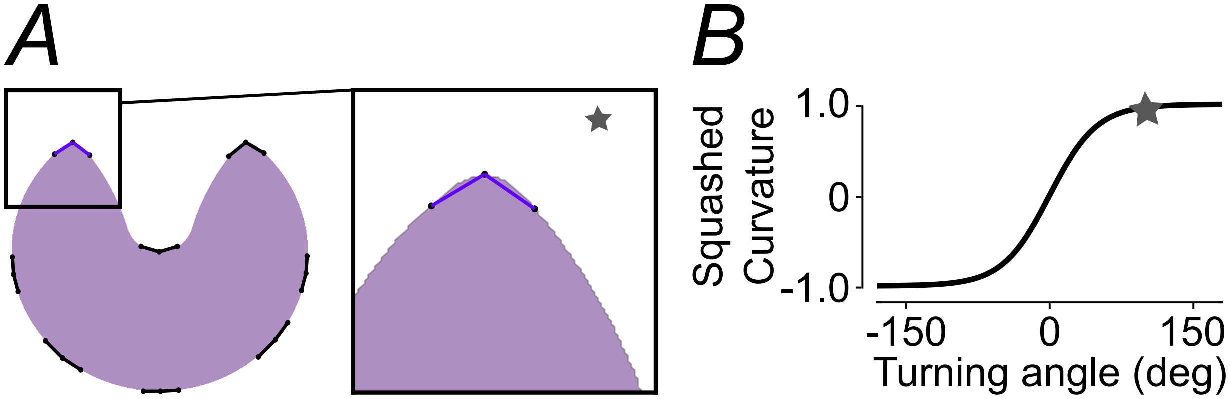

Figure 2.4: Shape discretization and curvature squashing. **A**, an example shape with 8 coordinates and vectors for tuning angle measurement. A convex feature is highlighted. **B**, the sigmoidal squashing function used to convert the tuning angles into curvature values between -1 and 1.

For each visually-responsive multi-unit site, the author constructed a 2-dimensional Gaussian function (Equation 1), in angular position and curvature space, using the neural responses to predict the response characteristics to a variety of shapes (Pasupathy and Connor, 2001). In Equation 2.2, β and α represent the offset and gain parameters used to map the arbitrary units back into interpretable units of spikes per second, respectively; x_c, x_a, σ_c, and κ are the parameters for the peak and spread of the curvature and angular position Gaussians. The author used Matlab's *lsqnonlin* optimization routine, an optimization routine that utilizes gradient descent to minimize a least squares error loss function, to calculate parameters for each multi-unit. Due to the non-convex nature of the optimization problem, demonstrated by the presence of many local minima, the author systematically sampled the initialization parameter space. Finally, the author determined the model parameters that produced the lowest error and therefore found the global minimum of the error surface for each multi-unit. In other words, these parameters produced a model prediction with the closest resemblance, both quantitatively and qualitatively, to the recorded neural responses. Further, the author used the model to predict the response to a given stimulus by selecting the maximum predicted response to all curvature and angular position pairs for a given stimulus (Figure 2.5D). The author visualizes this model using a 1-dimensional representation of a 2-dimensional Gaussian, where the darker color represents a bump in a plane or the peak of the Gaussian (Figure 2.5C). The drawn line denotes the angular position and curvature pairs of a shape stimulus in Figure 2.5D. The coordinates that lie near the peak of the Gaussian (point number 3), represents in dark purple, will be the decisive shape feature in predicting the response to a stimulus.

$$r_{apc}(\vec{x_c}, \vec{x_a}) = \beta + \alpha \cdot \left(max \left[e^{\frac{-(\vec{x_c} - \vec{\mu_c})^2}{\sigma_c^2}} \cdot \frac{e^{\frac{1}{\kappa} \cdot \frac{\cos \vec{x_a} - \vec{\mu_a}}{2\pi}}}{e^{\frac{1}{\kappa}}} \right] \right) \tag{2.2}$$

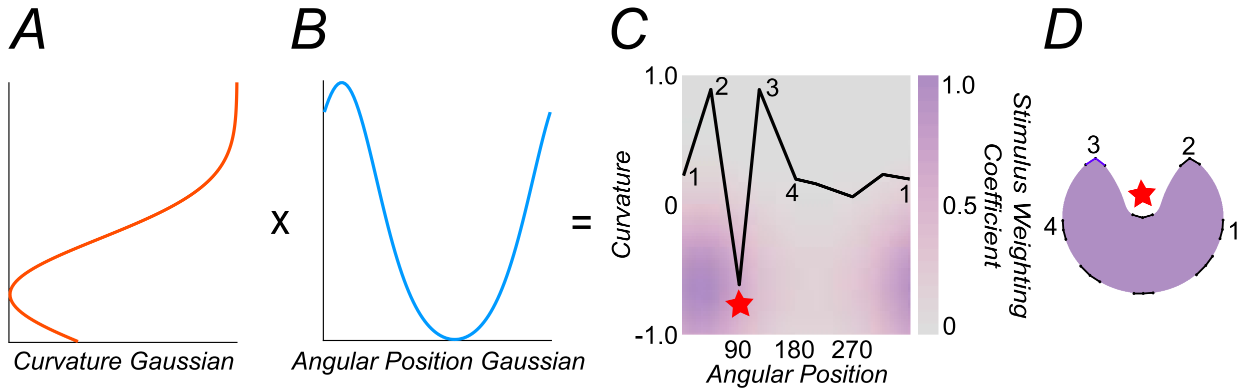

Figure 2.5: Construction of the angular position and curvature model. **A**, the model's Gaussian function in the curvature dimension. **B**, the model's angular position Gaussian for neural response prediction. **C, D**, a 2D representation of the APC model. The black line represents the angular position and curvature coordinates of the shape in **D**. The red star is the shape feature that will primarily be used for prediction since it lies closest to the peak of the multi-variable Gaussian.

The author made slight modifications to the Gaussian function proposed by Pasupathy and Connor (2001), by scaling the angular position Gaussian by its spread (κ), so that the amplitude of the function is always 1. This ensures that the gain and offset parameters have interpretable units in spikes per second, corresponding to the max baseline-subtracted response and spontaneous rate for a neuron, respectively.

2.2.3 Image-computable luminance (ICL) model

The author constructed an image computable luminance (ICL) model derived from the neural responses for each multi-unit site (Figure 2.6). The model consists of a linear combination of shape stimuli and their recorded neural responses normalized by the average expected image, which is an unweighted and normalized summation of the shape stimuli (Equation 2.3). The author used Matlab's *lsqnonlin* optimization routine to find values corresponding to the gain and offset parameters in order to map the arbitrary ICL units into units of spikes per second. Predicted responses consist of a stimulus (S) weighted by the image computable ICL model with applied gain (α) and offset (β) parameters for a given multi-unit site. S_i and r_i correspond to the *ith* stimulus and *ith* recorded response, respectively.

Since each pixel of the stimulus image is a parameter, the ICL model uses NxN + 2 parameters where the NxN represents the image computable model and the two additional gain and offset parameters. Importantly, much of the stimuli images are gray space that matches the color and luminance of the screen used for presentation. In other words, the true number of parameters is lower than the NxN + 2 estimate. The author rescaled the images to compare the performance of the ICL models with fewer parameters to that of the original ICL model (supplemental figure). Additionally, since we can decrease the number of ICL parameters to match the number of parameters in the APC model, we can make a comparison between the models that is not biased by the number of parameters. However, the model evaluation techniques in the next section prevent any issue related to the used parameter space, and therefore differences in the number of parameters cannot be the sole cause of increased performance.

$$r_{icl}(x_i\vec{m}g) = \beta + \alpha \cdot \left(\left[\frac{1}{N} \sum_{i=1}^{N} S_i \cdot r_i - \frac{1}{N} \sum_{i=1}^{N} S_i \right] \cdot S \right) \tag{2.3}$$

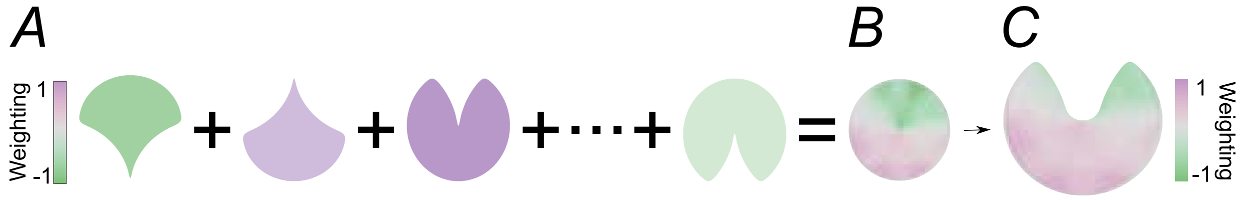

Figure 2.6: Construction of the image-computable luminance model. **A**, the shapes weighted by their responses. **B**, the ICL model is used to predict responses to shape presentation. **C**, a shape weighted by the ICL model and used to predict responses. Green represents inhibitory responses while purple represents excititory.

2.2.4 Model evaluation and comparison

The author implemented a k-fold cross-validation technique, to split the total shape set of stimuli into k training or testing sets. This technique ensures that each shape stimulus appears in the testing set once. Additionally, the author can determine whether models overfit using this approach. The author randomly selected and placed each stimulus into a single testing set so that we understand the effect of leaving out each stimulus on the performance and generalizability of the curvature and ICL models. The author used the same training and testing sets between the two models for the most equivalent comparison.

The author trained an individual model on each cross-validation training set and used the resulting parameters to predict the unseen data in the testing set. This measured the performance and generalizability of the model fits using variance-explained. This metric allows for a numerical interpretation of how well a model fits the data when compared to the mean. If a model just fits the mean of the data, we call this the null model since it predicts one value for all data points. Our variance-explained metric returns a value of 0 when the model produces a fit as good at explaining the data as the null model. We would consider this a poor fit since it cannot capture the characteristics of all the data points. As the variance explained value approaches 1, the ability to explain the variation within the data increases. A value of 1 corresponds to a perfect match between the recorded responses and the predictions. We consider a model to be generalizable when the testing variance explained is comparable to the training variance explained.

The author computed the variance explained for each training partition separately and averaged the values together to determine the overall training performance for each model (Equation 3). However, due to the small sample sizes in the testing sets per partition and the introduction of noise when dividing by a constant, the author computed the variance explained value for all testing sets together (Equation 4). The author found this method of calculating testing set variance explained returned values more representative and correlated with overall testing performance than calculating each partition's testing performance separately. Testing performance is the measure of the quality of fit. All the model performance values in the results are for the testing performance.

2.2.5 Shape space testing

VNL obtained single-unit neural data containing 109 well-isolated V4 neurons and their responses to 366 shapes (including orientation manipulations; 50 shapes without the orientation augmentation; Figure 2.7; Pasupathy and Connor, 2001). The author fit the curvature and ICL models to the single units and measured performance (see Methods: Model Evaluation and Comparison). To determine the ability of our limited shape set to capture shape selectivity, we extracted shapes from the larger shape set that were representative of the shape set used in the collection of the multi-unit data. We then trained both models with the reduced shape set and compared performance to the full model.

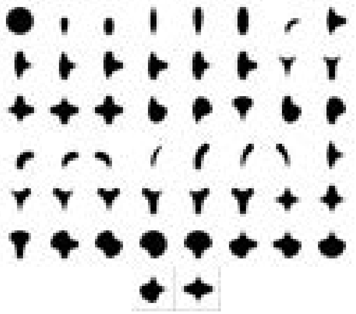

Figure 2.7: Expanded shape set used in Pasupathy and Connor, 2001. At all orientation presentations there are a total of 366 shapes

2.2.6 Multi-unit simulation

To understand the effect of different recording techniques on the model performance, the author constructed simulated multi-unit neurons by randomly selecting with replacement from the same 109 neurons used for the subset testing. This analysis assumes no underlying functional organization of V4 units. The author simulated sites constructed from a varying number of neurons

(2, 4, 6, or 8 neurons) as well as using different weighting factors for the contribution of a given site. A breakdown of the simulation points for the weighting factors are:

1. That neurons contribute equally and therefore all sites weighted equally
2. Neurons closer to the recording electrode contribute more
    (a) Neurons were randomly assigned weights so some sites contribute more to the response of the simulated multi-unit than others
    (b) Neurons were systematically assigned evenly-spaced weights simulating a gradual decrease in the contribution of sites where those further from the electrode would have a lower weighting factor.

The author then compared the performance of the models against the median performance value of the single-units used in the multi-unit construction to estimate if there were differences between the simulated sites and the neurons used to construct each multi-unit.

CHAPTER 3

RESULTS

Here, the author reports the results of an experiment to measure the developmental changes of shape selectivity across the ventral visual cortex. VNL presented stimuli previously used to understand size-invariant coding in V4 (El-Shamayleh and Pasupathy, 2016), at several orientations within the collective multi-unit receptive fields. The author used a well-studied model for curvature selectivity, referred to as the Angular-Position and Curvature (APC) model to characterize shape selectivity in our dataset. The author developed and implemented a simple image-computable luminance model and tested how well it explained neural responses in higher-order visual cortex. To account for experimental differences between our work and prior studies, we performed control analyses on a previously-published dataset of shape-selective V4 neurons (Pasupathy and Connor, 2001).

3.1 Changes in stimulus and orientation modulate responses

We used the shape stimulus set shown in to study the neural responses of multi-unit recordings within visual area V4. VNL presented each stimulus at several orientations within the collective multi-unit receptive fields. Each visually-responsive site responded uniquely to each presented stimulus. In order to understand the response differences between stimuli for a given neural site, the author plotted the response to several stimuli as a function of time, formally known as a peri-stimulus time histogram (PSTH). An example of a site with some example stimuli are shown in Figure 3.1A. Visually responsive sites showed modulation of response to the primary curvature component. Each site demonstrated a preference for a curvature feature based on the magnitude and type of primary boundary feature: convexity or concavity. Additionally, sites showed a diverse set of tuning properties. Some sites demonstrated modulated responses solely by orientation, where differently oriented augmentations of the same stimulus-evoked magnitude-varied activity (Figure 3.1A). To effectively visualize the response characteristics and differences across the stimulus and orientation space for a single multi-unit we organize the PSTHs in Figure 3.1B. Each tile represents the average response over a chosen time window of 200ms which covers stimulus presentation and interstimulus period shown in Figure 3.1A. As seen in the PSTHs, we see a preference in response across all stimuli and orientation presentations. This site demonstrates increased neural activity during the presentation of convex stimuli presented at 0° (to the right) and lesser magnitude responses to 90° and 180° oriented stimuli. This particular example shows responses with greater modulation to changes in orientation than the curvature feature.

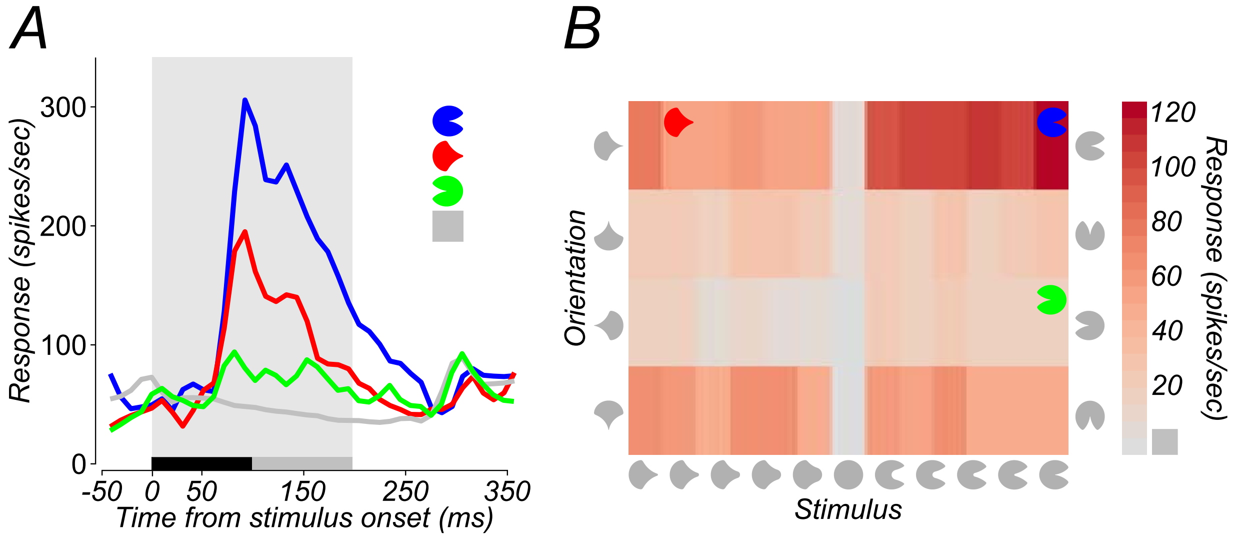

Figure 3.1: Change in response magnitude to stimulus and orientation presentations. **A**, peristimulus time histograms for several stimuli. Each line represents the stimulus that is matched in color. The light grey bar is the spontaneous rate of this neural unit. The black bar along the x-axis represents the stimulus presentation period and the grey bar is the interstimulus period. The grey area is the summation window for analysis. **B**, heatmap representing the complex shape tuning of a neural site. Colored shapes on the heatmap correspond to the baseline-subtracted PSTHs in **A**. This site demonstrates a strong orientation preference with a slight concave stimulus bias.

3.2 Models capture recorded multi-unit neural responses

The author used two models, the APC and image-computable luminance (ICL) model, to determine what characteristics of shape stimuli effectively capture the response characteristics of a given neural multi-unit (Figure 3.2A). A visualization of the models is shown in Figure 3.2B, E (see methods for more details). Both models successfully, and qualitatively captured the lawful response differences across both stimulus and orientation despite using vastly different methods (Figure 3.2C, F). Both models are capable of predicting the preference for concave stimuli at 45° and 90°, but the APC model is better able to capture the magnitude of the response.

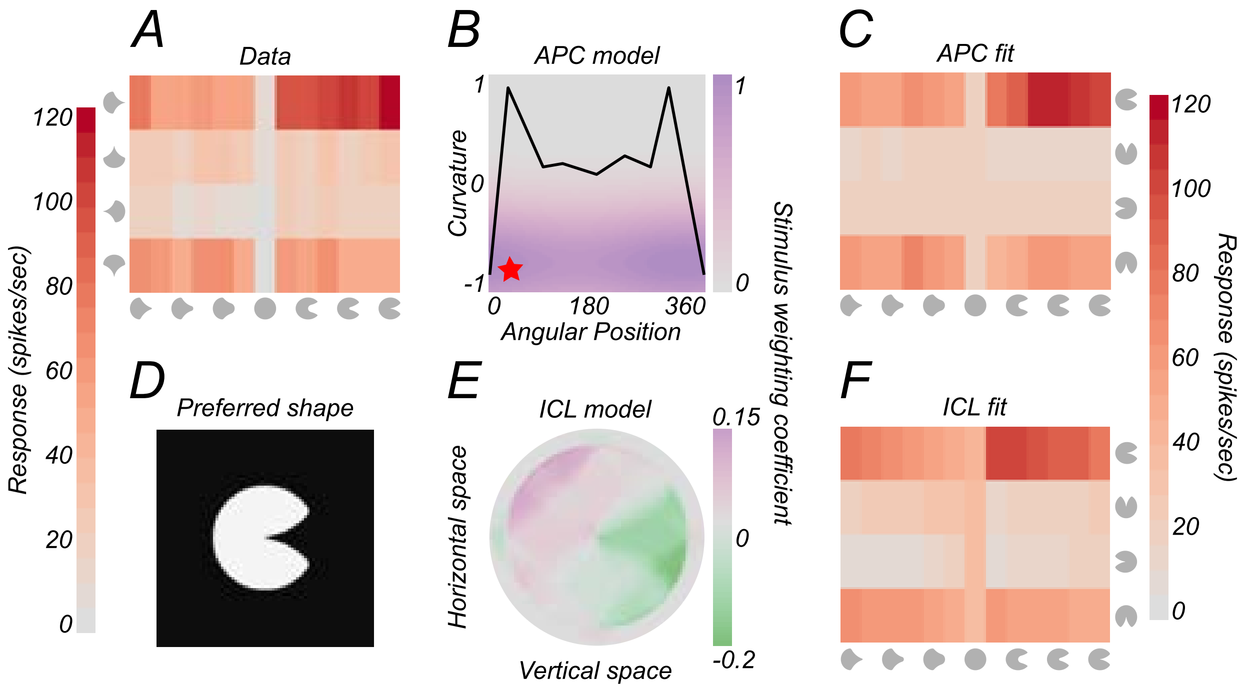

Figure 3.2: Models capture characteristics of neural responses. **A**, the heatmap representation of a multi-unit showing orientation and curvature tuning. The shapes on the x-axis are a few of the used stimuli, and the y-axis shapes are the 4 orientations used in stimulus presentation. **B**, APC model of the site in **A**. The black line corresponds to the preferred stimulus angular position and curvature coordinates; The predicting shape feature is highlighted by the red star. **C**, the APC model predicted responses to each stimulus and orientation pairing. Axes are the same as in **A**. **D**, the multi-unit's preferred stimulus, a concavity to the right (0°). **E**, the ICL model for the site in **A**. **F**, the ICL model predicted responses to all stimulus and orientation pairings; axes are the same as in **A**.

Regardless of the tuning characteristics of a given neural site, the models are able to accurately predict the responses in spikes per second, as seen by points scattered around the unity line in Figure 3.3. Recorded data values and predicted values for a monkey are quantitatively similar between models (Figure 3.3A, B, C, D). In order to determine an exact quantitative measure of similarity, we require a metric to differentiate between the models' ability to explain the recorded responses (see methods).

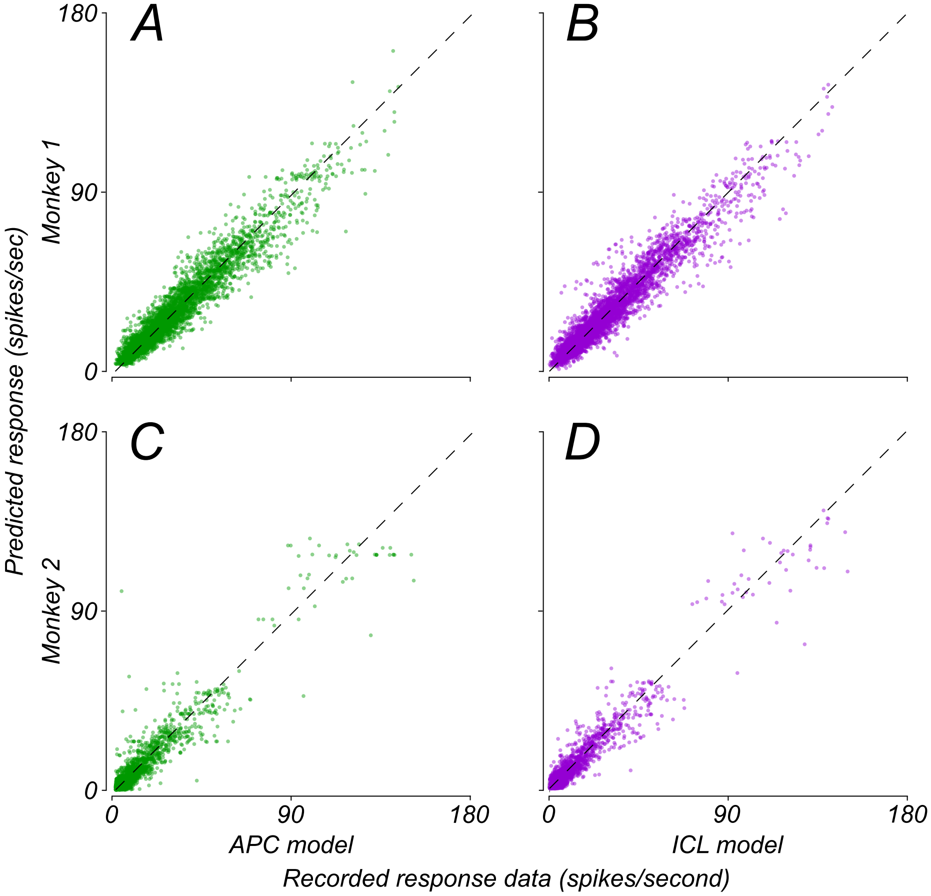

Figure 3.3: Models quantitatively capture neural responses across monkeys. **A, B** APC model fits to recorded V4 data in two monkeys. **C, D**, ICL model fits to recorded data in two monkeys. The dotted line presents the unity line. Points on this line are equal in predicted and recorded response values

3.3 Multi-unit model performance and comparison

To determine quantitative differences between the two models, the author implemented a variance explained (VE) measure to capture the quality of the fit for each neural site. A value of 0 VE corresponds to a fit as good as the mean of the data and a value of 1 VE corresponds to a fit where each recorded data point is perfectly predicted so that there is no error. The author only included sites that passed a split-half correlation cutoff. A small number of sites in V1 and IT were visually responsive (n = 12 and n = 11, respectively). A substantial number of sites in V2 and

V4 were visually responsive (n = 72 and n = 95, respectively). To visualize these differences on a per-site basis, we make a scatter plot where the x-axis represents the model performance in VE for the APC model and the y-axis represents the ICL model performance (Figure 3.4). The APC model explained the response variance ($r^2 > 0.1$) of many sites across V1, V2, V4, and IT (75%, 74%, 77%, and 100%, respectively). However, the ICL model explained a greater proportion of sites in V1, V2, and V4 (92%, 97%, and 92%, respectively). The ICL model explained the same proportion of sites in IT. The models could not explain a small proportion of sites in V2 and V4 (1% and 5%, respectively). However, the models simultaneously explained a large proportion of sites in these areas (72% and 75%). Figures Figure 3.3B and C demonstrate a graphical illusion. Of sites that are explainable by either model, there are a similar proportion of sites that lie below the dotted diagonal and therefore are better fit by the APC model ($V2_{APC}$ = 29%, $V4_{APC}$ = 32%). The ICL model explained a majority of sites that are fittable better than the APC model ($V2_{ICL}$ = 71%, $V4_{ICL}$ = 68%).

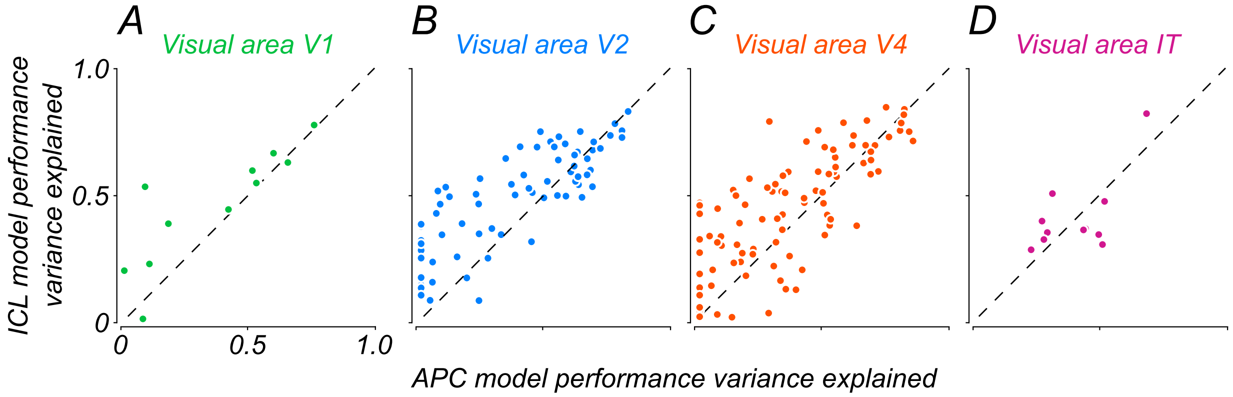

Figure 3.4: APC and ICL model performance for multi-unit data across the ventral visual pathway. **A**, is the comparison of the two models on fitting sites in V1. **B**, model comparison in V2. **C** model comparison in V4. **D**, model comparison in IT. All dots represent the variance explained values for each site. The dotted lines are the unity line and a point on this line represents a similar performance for both models.

3.4 Single-unit APC and ICL model performance and comparison

To account for experimental differences of recording technique and stimulus set in our work and previous work, the author performed control analyses on a previously-published dataset of well-isolated shape selective V4 single-units (Pasupathy and Connor, 2001). Previous work found that all 109 neurons were visually responsive, so the author did not exclude any sites from these analyses. Researchers used a larger stimulus set for data collection than used in the collection of our multi-unit data (Figure 3.5A). To visually and quantitatively compare the model performances of the APC and ICL models on the same single-units, we can use a scatter plot. Figure 3.5B shows a plot where the x-axis represents the model performance in VE of the APC model and the y-axis represents the model performance of the ICL model similar to that in Figure 3.4, which uses multi-unit with a limited shape set and Figure 3.5B uses single-unit data with a larger unconstrained shape set. The APC model explains about 74% of sites ($r^2 > 0.1$) while the ICL explains 82% of the sites. There are a few sites that either model cannot explain (9%). The APC model better explains more sites (54%; points that lie below the dotted diagonal than the ICL model (45%).

We observe similar trends between the two datasets despite differences in experimental designs. In both datasets, the ICL model explained a greater proportion of sites than the APC model and the models could not explain a small number of sites. However, there is a difference in the proportion of sites better fit by one model than the other. In the multi-unit data, the ICL model explained a greater number of sites than the APC model (Figure 3.4B, C) and in the single-unit data, the APC model better explains more neurons than the ICL model (Figure 3.5B). However, the differences in proportions are lesser than what we observed in the multi-unit data.

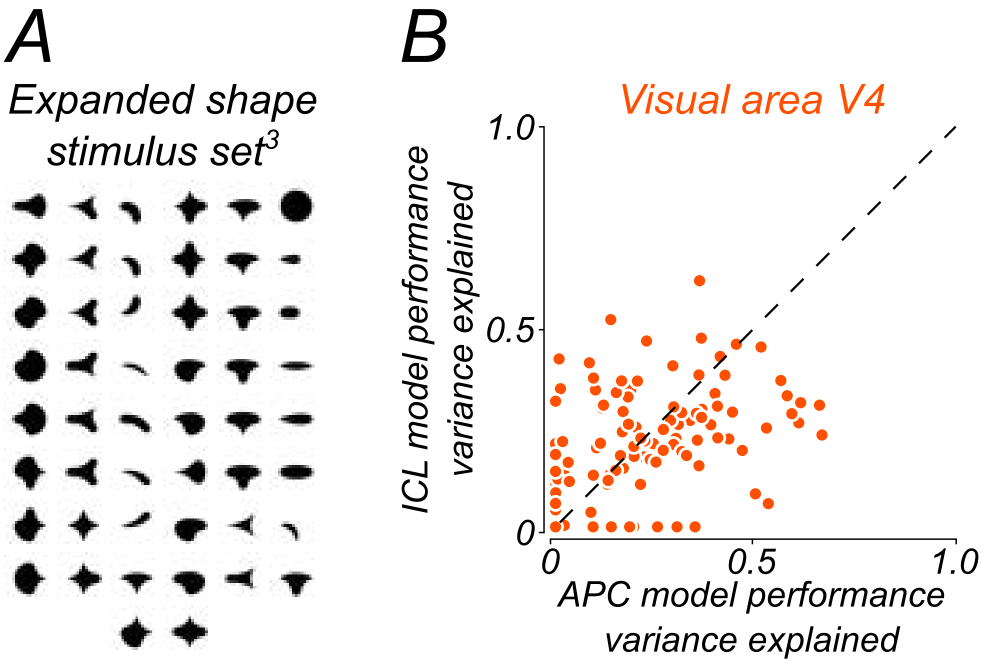

Figure 3.5: APC and ICL model performance for single-unit data. **A**, the shape set used in collecting single-unit data from Pasupathy and Connor, 2001. The shapes were presented at 2, 4, 6, or 8 orientations based on symmetry, resulting in 366 total stimuli. **B**, APC and ICL model comparison in variance explained for single-unit data. Points along the diagonal represent a similar performance by both models.

3.5 Stimulus set leads to decreased model performance

To determine whether any differences exist between the two datasets, the author explored the proportion of sites explained with a limited shape set. The author chose a limited shape set representative of the shapes in **Figure 1M** and tested how well the smaller subset of shapes generalizes to the rest of the shapes used in the larger shape set Figure 3.6B. To demonstrate if the representative shape set generalizes to other shapes better than a randomly selected subset, the author also determined the model performance when trained on a random subset (Figure 3.6A) and the full shape set from Pasupathy Connor (2001) (Figure 3.5A). The model performance for the full shape set, both trained and tested within, shows similar performance between both models ($median_{APC}$ = 0.20 VE, $median_{ICL}$ = 0.22 VE; Figure 3.6C). A large proportion of sites (45% APC; 75% ICL) perform better than the null model, those above the dotted line, for the representative subset. Overall, smaller proportions of sites generalize well for the random subset for both models (10% APC; 23% ICL) and the ICL model performs better, on average, than the APC model on both a random shape set ($median_{APC}$ = -0.3005 VE; $median_{ICL}$ = -.1178 VE). We observe the same trend in the models trained on the representative shape set ($median_{APC}$ = -0.0425 VE; $median_{ICL}$ = 0.1071 VE). Overall, the full shape performs the best on average, followed by the representative shape set, and then by the randomly selected shape subset.

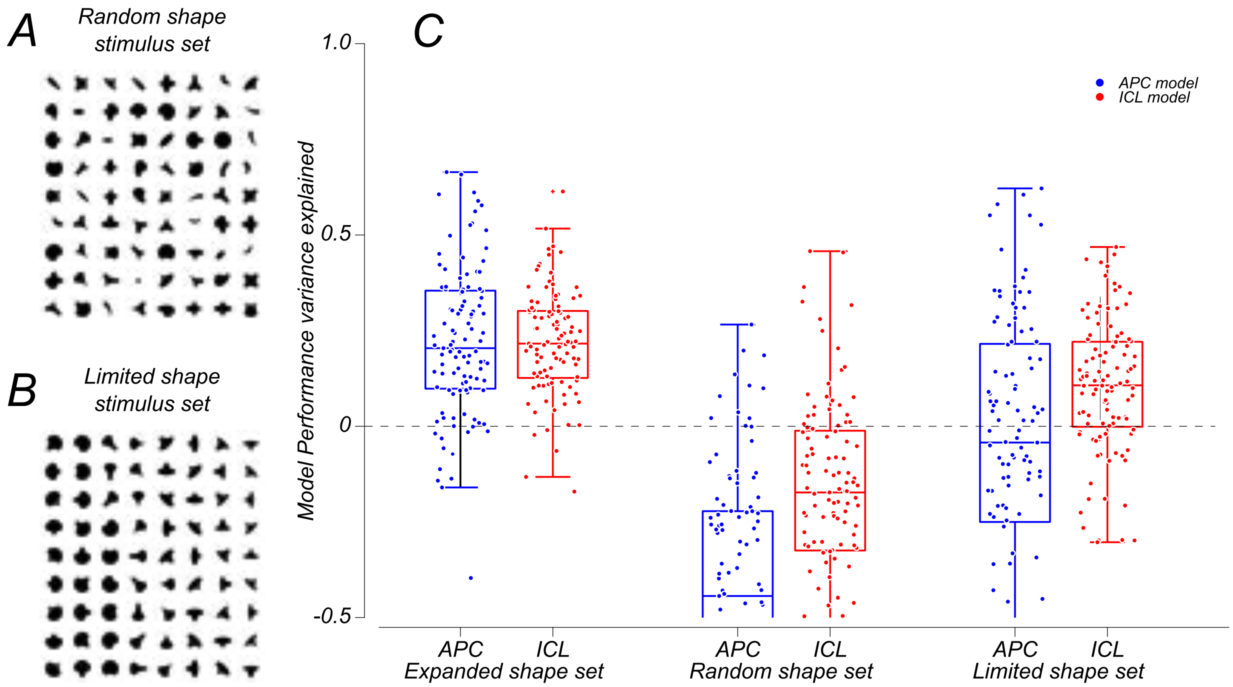

Figure 3.6: Generalizability of limited shape sets to expanded shape set. **A**, a random shape set derived from the expanded shape set used to determine the ability for a random shape subset to capture neural responses to stimuli outside the subset. **B**, a limited shape set representative of the shapes used in VNL's multi-unit recordings. **C**, distributions of the model performances in variance explained for both models across all shape sets: expanded, random, and limited representative.

When compared directly with the model performance on the full shape set, there is a similar performance between the representative reduced shape set and full shape set for both APC and ICL models (Figure 3.7). There are no sites that perform better when using a reduced shape set for the

APC model (Figure 3.7A). However, we observe a small proportion of sites better explained with a smaller shape set for the ICL model (20%; Figure 3.7B). The models could not explain about 24% of sites while the ICL could not explain about 12% using the same metric as used previously ($r^2 > 0.1$).

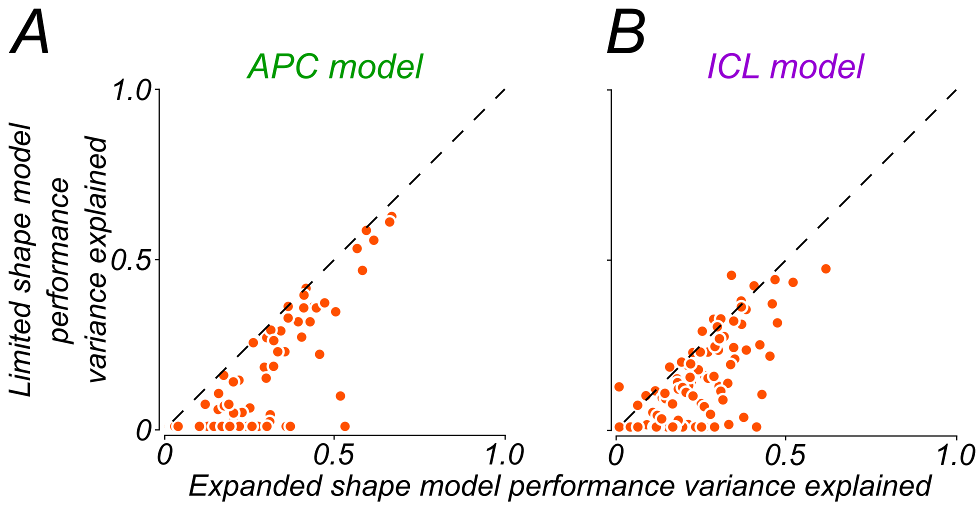

Figure 3.7: Comparison of full and limited shape APC and ICL models. **A**, the model comparison for the APC model. Sites below the dotted line are better explained using an expanded shape set. **B**, model comparison for the ICL model.

A comparison of the model performances on a limited shape set is shown in Figure 3.8. Many sites are similarly fit as demonstrated by the points around the dotted diagonal. The APC model explained 32% of the sites and the ICL model explained 53% of sites. The models were unable to explain 36% of the single units. About 44% (n = 30) of sites able to be fit by the models were better explained by the APC, while the ICL model better explained 56% (n = 38) of sites. We observed 11% of sites generalize with the APC model, but not the ICL model, and 32% generalize with the ICL model but not the APC model.

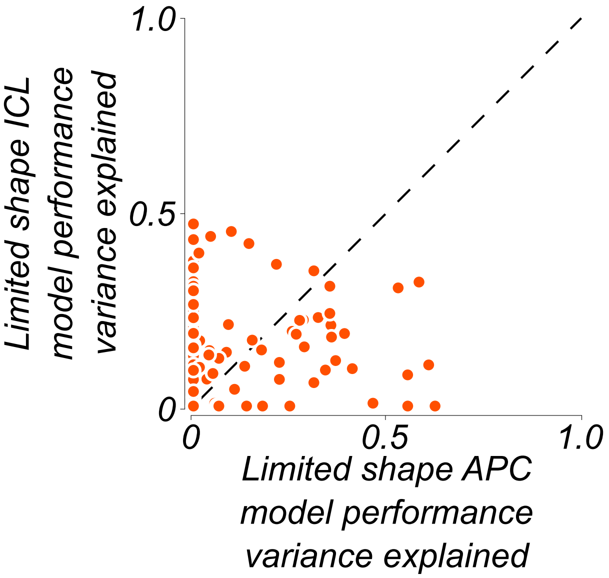

Figure 3.8: Model performance comparison of limited-representative shape sets for both models. Each point represents a single-unit plotted as its model performance on the limited shape APC and ICL models.

3.6 Recording technique has no impact on model performance

To determine whether the recording technique may affect the ability of the models to capture the responses, the author constructed simulated multi-unit sites using a 4x3 construction design. To measure whether the recording strategy affects model performance, the author compared the simulated multi-unit performance to the median performance value of its constituent single-units. The number of units used to construct each simulated multi-unit does not have an effect on the ability of the APC model to explain the responses, as demonstrated by sites clustered around the dotted-diagonal (Figure 3.9A). We observe similar trends in the ICL model for the simulated multi-units(Figure 3.9C). The ICL model explains the simulated multi-units and their average single-unit constituent unit comparably. The different single-unit weighting techniques also do not have an effect on the performance of the models (Figure 3.9B, D).

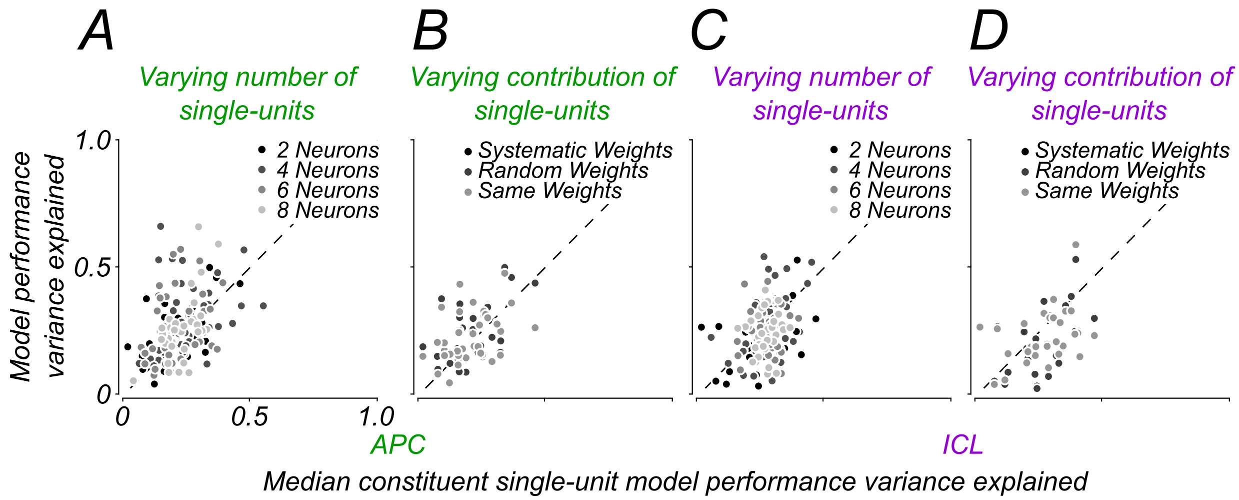

Figure 3.9: Simulated multi-unit performance. **A**, APC model performance of simulated multi-units compared to the median performance of single-units used in multi-unit construction. **B**, APC model performance using different single-unit contribution weighting techniques. **C**, ICL model performance of simulated multi-units compared to the median performance of single-units used in multi-unit construction. **D**, ICL model performance using different single-unit contribution weighting techniques.

3.7 Shape selectivity tuning widths are stable during development

Lastly, to determine if shape selectivity tuning widths change with age, the author measured the APC model parameters for curvature and angular position tuning widths for our recorded multi-unit data at two age points. The width values have arbitrary units. The curvature width of the shape tuning is stable across age as determined by median value ($curvWidth_{7months}$ = 0.449, $curvWidth_{12months}$ = 0.442; Figure 3.10A). There is a slight sharpening of the angular position width from 7 months ($angWidth_{7months}$ = 1.08) to 12 months ($curvWidth_{12months}$ = 0.609) (Figure 3.10B).

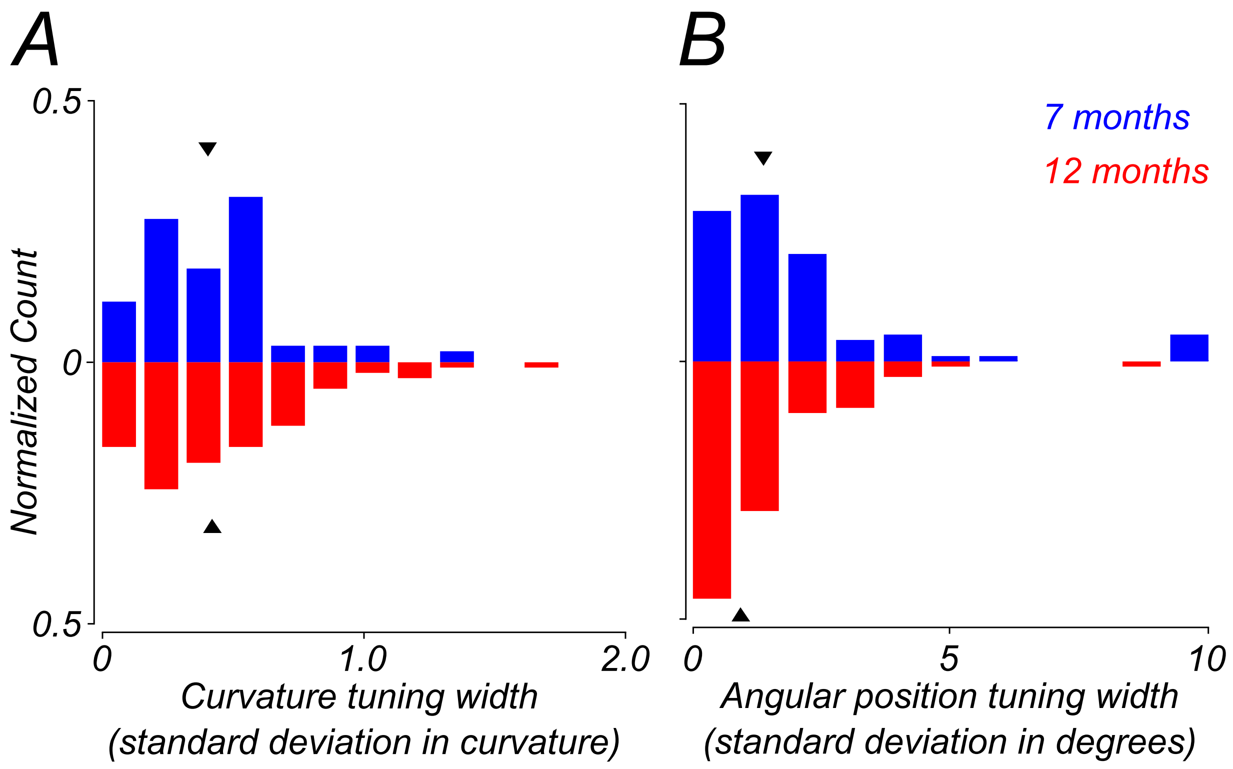

Figure 3.10: Comparison of shape tuning bandwidths across age. **A**, the curvature tuning width for 7 and 12 months. The triangle represents the median of the distributions for both ages. **B**, the angular position bandwidth distributions at both recorded ages. Triangles represent the medians of the distributions.

CHAPTER 4

DISCUSSION

To examine the developmental basis of shape selectivity in primate ventral visual pathway, we asked whether a classical APC model and a local stimulus luminance model can explain neural response modulation by both curvature and orientation. The author found both models explain a large proportion of sites across several visual areas. Noticeably, we observed similar proportions of V2 and V4 units explained by the models. To further draw connections between our dataset of multi-unit recordings with a smaller stimulus set, the author ran control analyses on well-isolated single-unit V4 neurons. We observed similar trends between the single-unit data and our recorded multi-unit data. The author found that a limited shape set generalizes to a larger shape set in a proportion of sites. Additionally, the recording technique did not impact the ability of the models to explain the data. Collectively, these findings suggest that there is substantial shape information that is contained within the neural data prior to visual area V4, experimental design differences do not affect the ability of the ICL model to explain responses in visual areas, our multi-unit data is sufficient to study development, and that the tuning widths of shape features are stable from 7 to 12 months.

4.1 Modulated responses in visual area V4

As expected, we found a modulation of response by both curvature feature and orientation of a stimulus in ventral visual area V4 as shown in Figure 3.1. This demonstrates classical shape selectivity and agrees with previous shape selectivity studies in macaque V4 neurons with a variety of stimuli constructions (Carlson et al., 2011; El-Shamayleh and Pasupathy, 2016; Pasupathy and Connor, 1999, 2001). The presence of shape modulation supports the use of multi-unit, or population, recordings to study shape selectivity in cortex. While this is not surprising, it is important to confirm due to the lack of studies that use this recording strategy. Additionally, we found the multi-units preferred acute curvatures, such as strong concavities and convexities, agreeing with previous work by Carlson et al. (2011) despite the differences in stimulus design.

4.2 Models capture recorded multi-unit neural responses

As expected, we are able to capture the responses of V4 multi-units with the APC model. In other words, the responses to a given shape could be accurately predicted using the curvature and angular position values of a shape boundary element (Figure 3.2C). However, contrary to expectation, the ICL model also qualitatively described the response properties to a given shape (Figure 3.2F). We expected the ICL to perform poorly and act as a baseline for the shape information captured by early visual structures but instead observed a large amount of the response accurately predicted (Figure 3.3).

4.3 Multi-unit model performance and comparison

Since it was unclear how well these models quantitatively compared in the ability to capture the responses, the author calculated the explained variance of each fit. Unexpectedly, we saw that both models were successful in predicting a large proportion of sites across the ventral stream rather than just visual area V4 (Figure 3.4). Since shape selectivity, as described by the angular position and curvature features of a shape, is thought to arise in V4, we expected the APC model to explain few sites in earlier visual areas. Additionally, as mentioned before, we expected the ICL model to perform poorly across all visual areas due to its luminance-based construction. However, the performance comparisons in V1 and IT require more recordings due to the small sample size of visually responsive sites and therefore we should be careful when making conclusions about the ability of the models to capture responses in either area. Our sample of sites in V1 and IT are well explained by both models, but may not represent the characteristics of a population of sites from those areas. Both models explained a large proportion of sites in visual area V2. Due to previous work (Pasupathy and Connor, 2001) that successfully modeled responses in V4 with the APC model, we expected that the shape information properties of curvature and angular position likely emerged in V4, not V2. However, the presence of many sites well-described by the APC model in V2 suggests that shape processing emerges before V4. Largely, this parallels previous studies conducted in V2; however, the capabilities for shape processing far exceed previous expectations (Hegdé and Van Essen, 2000). Due to the stimuli differences between this work and previous work in V2 for studying shape processing, this suggests that future work in V2 can use the APC model as a tool. Aligning with expectations, we observed a large number of sites well captured in V4, agreeing with previous work despite the differences in experimental design (Pasupathy and Connor, 2001).

As seen in both V2 and V4, the luminance-based ICL model outperformed expectations. We expected to see model performance be at or below 0, indicating worse performance than the null model, across all cortical areas. However, we witnessed that local stimulus luminance explained a greater proportion of sites than the angular position and curvature-dependent predictions in V2 and V4. This suggests that luminance may play an important role in higher-visual cortex processing. We did not expect this result since previous work found that computations in earlier visual areas (V1 and V2) contain nonlinearities. (Movshon et al., 1978a, 1978b). The ICL model represents linear processing and therefore we thought it would be too simple to extract meaningful information for response prediction. We also observed a large proportion of sites better explained by the ICL model than the APC model. We expected many sites would be better explained by the APC model in V4, due to the concept, as mentioned before, that shape selectivity arises in V4 (Pasupathy and Connor, 1999, 2001). However, as mentioned earlier, we found the opposite of what we expected.

Our experiment and previous work used vastly different experimental designs and we required analyses to understand the impacts of each difference. While we used multi-unit recordings, which precludes isolation of the responses of individual neurons without complication analysis, previous work used well-isolated single-unit V4 recordings (Pasupathy and Connor, 2001). Additionally, our work uses a smaller shape set than that used in the collection of single-unit data. These experimental differences could potentially cause these discrepancies and motivate the next analyses performed. Subsequently, we turned to previously recorded datasets that use different recording strategies to study shape selectivity to understand the impact of our experimental construction on model performance.

4.4 Single-unit model performance and comparison

Initially, we obtained well-isolated single-unit V4 data from Pasupathy Connor (2001) used to propose the APC model for shape selectivity. We fit both models to the data, using the entire shape set to train the model, and compared the amount of the explained variance on a per-site basis (Figure 3.5). Surprisingly, we found a similar trend to our data in V4 (Figure 3.4C). We expected that the ICL model would be unable to explain many sites, but found that the model explained a greater proportion of sites than the APC model. Importantly, the presence of ICL explainable units in a different dataset, and the similarities in trends between model performance comparison, confirm that the ICL model is capturing information important for shape processing and that the experimental choices do not impact the model's success.

In contrast with our data, we see a larger proportion of sites better explained by the APC model than the ICL model. However, the potentially-biased collection strategies used in the single-unit recordings, where sites were only recorded only if they demonstrated shape-modulated responses, provide a plausible explanation for the proportion differences observed in the multi-unit and single-unit data. The selection process may have unknowingly discarded many sites that would be better explained using the ICL model. Future studies are necessary to elucidate this potential difference.

Importantly, the similar performance measures between our data and the single-unit dataset suggest that we can use the multi-unit data for future developmental studies. Since the APC model is well-studied, it is our best tool for determining whether differences in our limited set or recording strategy are responsible for the discrepancies between the two datasets. If there are no concerns, we can explore whether neural representations of shape change during the first year of life.

4.5 Stimulus set size control

In order to effectively understand how our experimental design affects APC performance, we compared the performance of 3 APC models: one trained on the full shape set, one trained on a random subset of shapes from the larger shape set, and one trained on a shape set representative of the shape set used in our multi-unit recordings (Figure 3.5A; Figure 3.6A, B). The larger stimulus set contains stimuli with several convex projections and therefore more complex shapes. By isolating the representative subset, we can conclude whether our shape set is sufficient to study shape selectivity. We found that a representative shape set was able to better generalize to a diverse stimulus set than the random subset on average (Figure 3.6C). This is not particularly surprising as the representative shape set contains all shapes at their presented orientations, and tiles the shape space, while the random set may only contain a shape at one or a few orientations. This suggests that the chosen stimulus set used in our experiment is better suited for a shape-selectivity experiment than a randomly chosen one. However, we do see decreased APC model performance compared to the ICL model with the random and representative subsets, indicating that the APC model is most successful with an expansive shape set (Figure 3.6). This could explain the differences in the proportion of sites better explained by the ICL model in our data and the single-unit data since we use a limited shape set. However, the current analysis uses shapes in 8 orientations, not 4, so future analysis is necessary to understand the true magnitude of decreased APC model performance. However, in agreement with previous analyses, the limited shape set is not the cause of ICL model success since the full shape set is similarly explained by both models (reffig:fifthRFig, Figure 3.6).

The comparisons between the full and reduced shape set for both models is better represented by Figure 3.7. We can see in the comparison of the two shape sets and the APC model that there are many sites that are comparably fit by both shape sets. However, the limited shape set could not explain a proportion of sites. We observed similar trends in the ICL model comparison. This demonstrates that our limited shape set is only able to capture a proportion of sites, but we require further analysis to establish characteristics that aid in the explainability. Interestingly, this trend is present for both models which deters any suspicions of the shape set being responsible for the ICL performance in our data. If the opposite were true, we would expect the ICL model performance to increase with the use of a smaller stimulus set. However, there are a few sites that seem to be better explained with a reduced shape set ICL model. Since the difference is quite small, the limited shape set does not lead to overall increased ICL performance.

After comparing the subset shape set models to the full models, we compared the subset APC and ICL models against each other (Figure 3.8). As before, many of the sites lie around the diagonal and represent a similar performance for both models. However, for the first time, we see the emergence of a large proportion of sites that lie along the y-axis. These sites represent single-units explainable by the ICL model, but not the APC model. This shows that many of the multi-unit sites in our data are capable of being explained by the APC model with fewer shapes since we have explained variance values much greater than those in the shape subset control on single-unit data. Further, this demonstrates that the APC model's performance decreases when using a smaller shape set and the ICL model performance is relatively unchanged for most sites. As stated before, this finding suggests that the limited shape set caused the model performance discrepancies between our dataset and the single-unit dataset. However, the limited shape set only decreases APC performance and does not increase ICL performance for most sites.

4.6 Simulated multi-unit model performance and comparison

To make sure that the recording differences between our work and previous work had no bearing on the APC or ICL explainability, we simulated multi-unit sites using the well-isolated single units. Regardless of the construction technique, the performances of both models were largely scattered around the diagonal representing a comparable performance to the median performance of the units used in construction (Figure 3.9). These findings match expectations and are important for confirming that our recording technique has no impact on performance or the trends we observed. Specifically, the number of neurons used to construct our multi-units did not obviously affect performance and the weighting technique did not influence the ability of the models to explain the sites. This agrees with the similarity of trends observed between the two datasets where the model performance did not drastically decrease when using single-unit data. Importantly, our construction technique does not take any spatial organization assumptions into account, which may be the opposite of what is true in V4. Many other areas show distinct spatial arrangements of orientation or monocular input. Therefore, the potential presence of curvature organization in V4 is not surprising. However, our observation in a randomized construction of sites would not likely change if we understood the spatial layout of neurons in V4.

4.7 Stable shape selectivity parameters during development

Since we have performed extensive analyses to show that the APC model explains our data, we used the model as a tool for studying the development of shape selectivity (Figure 3.10). We expected that the tuning widths of the curvature and angular position parameters of the model to be stable across development from age 7 to 12 months due to similar results with other visual functions in other visual areas. Our findings agree with our expectations and previous work completed in behavioral tasks and in physiological studies of area IT (Kiorpes, 2016; Rodman et al., 1993). The small difference in the median value in the angular position tuning width requires more analysis to understand whether the change is significant (Figure 3.10B). Since this is the first study of developmental shape selectivity in V4, we cannot make comparisons to the development of visual functions of V4, but our findings suggest that shape selectivity in V4 is fully mature by age 7 months in *Macaca nemestrina*.

CHAPTER 5

CONCLUSION

This study examined the ability for a luminance-based model to capture neural responses in visual cortex and how shape selectivity develops from 7 to 12 months in monkeys. We found that a novel image computable luminance model is able to explain a large proportion of sites and in some cases better than the APC model. This implies that luminance plays a crucial role in the processing occurring in higher-visual cortex. Additionally, APC and ICL models were able to explain sites in visual area V2 during the presentation of shape stimuli suggesting that shape selectivity emerges in V2 and not V4. Also, we found evidence for stable development of shape selectivity after 7 months of age, indicating a mature V4 as early as 7 months in monkeys or 2.5 years in humans. This implies that the onset of a developmental disorder like amblyopia after this age point will have little effect on an individual's shape-processing abilities. Due to control analyses performed on a single-unit dataset collected from previous work, we can conclude that our experimental differences do not pose any issues related to the observations for both APC and ICL model performance as well as development. However, the APC model cannot explain sites as well with a limited stimulus set than an extensive set. In other words, we can study shape selectivity and development with our data and future datasets using a similar paradigm. In the future, the use of a larger stimulus set is a better choice when studying shape selectivity in V4, especially if the researchers plan to use the APC model. Overall, the modeling and analysis of shape selectivity, both in adulthood and development, allows for a nuanced understanding of the processing that may occur within visual areas so that clinicians can implement effective preventative or rehabilitative strategies for visual conditions.

REFERENCES

Alonso, J.-M., & Martinez, L. M. (1998). Functional connectivity between simple cells and complex cells in cat striate cortex [Number: 5 Publisher: Nature Publishing Group]. *Nature Neuroscience*, *1*(5), 395–403. https://doi.org/10.1038/1609

Attebo, K., Mitchell, P., Cumming, R., Smith, W., Jolly, N., & Sparkes, R. (1998). Prevalence and causes of amblyopia in an adult population. *Ophthalmology*, *105*(1), 154–159. https://doi.org/10.1016/S0161-6420(98)91862-0

Bear, M. F., Connors, B. W., & Paradiso, M. A. (2016). *Neuroscience: Exploring the brain* (Fourth edition). Wolters Kluwer.

Blakemore, C., & Vital-Durand, F. (1986a). Effects of visual deprivation on the development of the monkey's lateral geniculate nucleus. [_eprint: https://onlinelibrary.wiley.com/doi/pdf/10.1113/jphysiol.198 *The Journal of Physiology*, *380*(1), 493–511. https://doi.org/10.1113/jphysiol.1986.sp016298

Blakemore, C., & Vital-Durand, F. (1986b). Organization and post-natal development of the monkey's lateral geniculate nucleus. *The Journal of Physiology*, *380*, 453–491. Retrieved March 15, 2023, from https://www.ncbi.nlm.nih.gov/pmc/articles/PMC1182949/

Blasdel, G., Obermayer, K., & Kiorpes, L. (1995). Organization of ocular dominance and orientation columns in the striate cortex of neonatal macaque monkeys. *Visual Neuroscience*, *12*(3), 589–603. https://doi.org/10.1017/s0952523800008476

Boothe, R. G., Dobson, V., & Teller, D. Y. (1985). Postnatal development of vision in human and nonhuman primates. *Annual Review of Neuroscience*, *8*(1), 495–545. https://doi.org/10.1146/annurev.ne.08.030185.002431

Brackbill, N., Rhoades, C., Kling, A., Shah, N. P., Sher, A., Litke, A. M., & Chichilnisky, E. (2020). Reconstruction of natural images from responses of primate retinal ganglion cells (M. Meister, J. I. Gold, & H. Asari, Eds.) [Publisher: eLife Sciences Publications, Ltd]. *eLife*, *9*, e58516. https://doi.org/10.7554/eLife.58516

Cadieu, C., Kouh, M., Pasupathy, A., Connor, C. E., Riesenhuber, M., & Poggio, T. (2007). A model of v4 shape selectivity and invariance. *Journal of Neurophysiology*, *98*(3), 1733–1750. https://doi.org/10.1152/jn.01265.2006

Carlson, E. T., Rasquinha, R. J., Zhang, K., & Connor, C. E. (2011). A sparse object coding scheme in area v4. *Current Biology*, *21*(4), 288–293. https://doi.org/10.1016/j.cub.2011.01.013

Chino, Y. M., Iii, E. L. S., Hatta, S., & Cheng, H. (1997). Postnatal development of binocular disparity sensitivity in neurons of the primate visual cortex [Publisher: Society for Neuroscience Section: Articles]. *Journal of Neuroscience*, *17*(1), 296–307. https://doi.org/10.1523/JNEUROSCI.17-01-00296.1997

Clarke, W. N. (1999). Common types of strabismus. *Paediatrics & Child Health*, *4*(8), 533–535. Retrieved January 22, 2023, from https://www.ncbi.nlm.nih.gov/pmc/articles/PMC2830773/

DeAngelis, G. C., Ohzawa, I., & Freeman, R. D. (1995). Receptive-field dynamics in the central visual pathways. *Trends in Neurosciences*, *18*(10), 451–458. https://doi.org/10.1016/0166-2236(95)94496-R

DiCarlo, J. J., & Cox, D. D. (2007). Untangling invariant object recognition [Publisher: Elsevier]. *Trends in Cognitive Sciences*, *11*(8), 333–341. https://doi.org/10.1016/j.tics.2007.06.010

DiCarlo, J. J., Zoccolan, D., & Rust, N. C. (2012). How does the brain solve visual object recognition? *Neuron*, *73*(3), 415–434. https://doi.org/10.1016/j.neuron.2012.01.010

El-Shamayleh, Y., Kumbhani, R. D., Dhruv, N. T., & Movshon, J. A. (2013). Visual response properties of v1 neurons projecting to v2 in macaque. *The Journal of Neuroscience*, *33*(42), 16594–16605. https://doi.org/10.1523/JNEUROSCI.2753-13.2013

El-Shamayleh, Y., & Pasupathy, A. (2016). Contour curvature as an invariant code for objects in visual area v4 [Publisher: Society for Neuroscience Section: Articles]. *Journal of Neuroscience*, *36*(20), 5532–5543. https://doi.org/10.1523/JNEUROSCI.4139-15.2016

Eustis, S., & Smith, D. R. (1987). Parental understanding of strabismus [Publisher: SLACK Incorporated]. *Journal of Pediatric Ophthalmology & Strabismus*, *24*(5), 232–236. https://doi.org/10.3928/0191-3913-19870901-08

Fawcett, S. L., Wang, Y.-Z., & Birch, E. E. (2005). The critical period for susceptibility of human stereopsis. *Investigative Ophthalmology & Visual Science*, *46*(2), 521–525. https://doi.org/10.1167/iovs.04-0175

Freeman, J., Ziemba, C. M., Heeger, D. J., Simoncelli, E. P., & Movshon, J. A. (2013). A functional and perceptual signature of the second visual area in primates. *Nature neuroscience*, *16*(7), 974–981. https://doi.org/10.1038/nn.3402

Fujita, I. (2002). The inferior temporal cortex: Architecture, computation, and representation. *Journal of Neurocytology*, *31*(3), 359–371. https://doi.org/10.1023/A:1024138413082

Gross, C. G., Bender, D. B., & Rocha-Miranda, C. E. (1969). Visual receptive fields of neurons in inferotemporal cortex of the monkey. *Science (New York, N.Y.)*, *166*(3910), 1303–1306. https://doi.org/10.1126/science.166.3910.1303

Gross, C. G. (2002). Genealogy of the ”grandmother cell”. *The Neuroscientist: A Review Journal Bringing Neurobiology, Neurology and Psychiatry*, *8*(5), 512–518. https://doi.org/10.1177/107385802237175

Harwerth, R. S., Smith, E. L., Crawford, M. L. J., & von Noorden, G. K. (1990). Behavioral studies of the sensitive periods of development of visual functions in monkeys. *Behavioural Brain Research*, *41*(3), 179–198. https://doi.org/10.1016/0166-4328(90)90107-P

Hawken, M. J., Blakemore, C., & Morley, J. W. (1997). Development of contrast sensitivity and temporal-frequency selectivity in primate lateral geniculate nucleus. *Experimental Brain Research*, *114*(1), 86–98. https://doi.org/10.1007/PL00005626

Hegdé, J., & Van Essen, D. C. (2000). Selectivity for complex shapes in primate visual area v2. *The Journal of Neuroscience: The Official Journal of the Society for Neuroscience*, *20*(5), RC61. https://doi.org/10.1523/JNEUROSCI.20-05-j0001.2000

Holmes, J. M., & Clarke, M. P. (2006). Amblyopia. *The Lancet*, *367*(9519), 1343–1351. https://doi.org/10.1016/S0140-6736(06)68581-4

Hubel, D. H., & Wiesel, T. N. (1959). Receptive fields of single neurones in the cat’s striate cortex. *The Journal of Physiology*, *148*(3), 574–591. Retrieved March 15, 2023, from https://www.ncbi.nlm.nih.gov/pmc/articles/PMC1363130/

Hubel, D. H., & Wiesel, T. N. (1962). Receptive fields, binocular interaction and functional architecture in the cat’s visual cortex. *The Journal of Physiology*, *160*(1), 106–154.2. Retrieved February 11, 2023, from https://www.ncbi.nlm.nih.gov/pmc/articles/PMC1359523/

Hubel, D. H., & Wiesel, T. N. (1963). Receptive fields of cells in striate cortex of very young, visually inexperienced kittens [Publisher: American Physiological Society]. *Journal of Neurophysiology*, *26*(6), 994–1002. https://doi.org/10.1152/jn.1963.26.6.994

Kafaligonul, H., Breitmeyer, B. G., & Öğmen, H. (2015). Feedforward and feedback processes in vision. *Frontiers in Psychology*, *6*. Retrieved March 7, 2023, from https://www.frontiersin.org/articles/10.3389/fpsyg.2015.00279

Kim, U. S., Mahroo, O. A., Mollon, J. D., & Yu-Wai-Man, P. (2021). Retinal ganglion cells—diversity of cell types and clinical relevance. *Frontiers in Neurology*, *12*. Retrieved February 11, 2023, from https://www.frontiersin.org/articles/10.3389/fneur.2021.661938

Kiorpes, L. (2016). The puzzle of visual development: Behavior and neural limits [Publisher: Society for Neuroscience Section: Viewpoints]. *Journal of Neuroscience*, *36*(45), 11384–11393. https://doi.org/10.1523/JNEUROSCI.2937-16.2016

Kiorpes, L. (2019). Understanding the development of amblyopia using macaque monkey models [Publisher: Proceedings of the National Academy of Sciences]. *Proceedings of the National Academy of Sciences*, *116*(52), 26217–26223. https://doi.org/10.1073/pnas.1902285116

Kiorpes, L. (2015). Visual development in primates: Neural mechanisms and critical periods [_eprint: https://onlinelibrary.wiley.com/doi/pdf/10.1002/dneu.22276]. *Developmental Neurobiology*, *75*(10), 1080–1090. https://doi.org/10.1002/dneu.22276

Loudon, S. E., & Simonsz, H. J. (2005). The history of the treatment of amblyopia [Publisher: Taylor & Francis _eprint: https://doi.org/10.1080/09273970590949818]. *Strabismus*, *13*(2), 93–106. https://doi.org/10.1080/09273970590949818

Majaj, N. J., Hong, H., Solomon, E. A., & DiCarlo, J. J. (2015). Simple learned weighted sums of inferior temporal neuronal firing rates accurately predict human core object recognition performance [Publisher: Society for Neuroscience Section: Articles]. *Journal of Neuroscience*, *35*(39), 13402–13418. https://doi.org/10.1523/JNEUROSCI.5181-14.2015

Maruko, I., Zhang, B., Tao, X., Tong, J., Smith, E. L., & Chino, Y. M. (2008). Postnatal development of disparity sensitivity in visual area 2 (v2) of macaque monkeys [Publisher: American Physiological Society]. *Journal of Neurophysiology*, *100*(5), 2486–2495. https://doi.org/10.1152/jn.90397.2008

Morishita, H., & Hensch, T. K. (2008). Critical period revisited: Impact on vision. *Current Opinion in Neurobiology*, *18*(1), 101–107. https://doi.org/10.1016/j.conb.2008.05.009

Motlagh, M., & Geetha, R. (2022). Physiology, accommodation. In *StatPearls*. StatPearls Publishing. Retrieved January 22, 2023, from http://www.ncbi.nlm.nih.gov/books/NBK542189/

Movshon, J. A., Thompson, I. D., & Tolhurst, D. J. (1978a). Receptive field organization of complex cells in the cat's striate cortex. *The Journal of Physiology*, *283*, 79–99. https://doi.org/10.1113/jphysiol.1978.sp012489

Movshon, J. A., Thompson, I. D., & Tolhurst, D. J. (1978b). Spatial summation in the receptive fields of simple cells in the cat's striate cortex. *The Journal of Physiology*, *283*, 53–77. Retrieved January 19, 2023, from https://www.ncbi.nlm.nih.gov/pmc/articles/PMC1282765/

Movshon, J. A., Kiorpes, L., Hawken, M. J., & Cavanaugh, J. R. (2005). Functional maturation of the macaque's lateral geniculate nucleus [Publisher: Society for Neuroscience Section:

Behavioral/Systems/Cognitive]. *Journal of Neuroscience*, *25*(10), 2712–2722. https://doi.org/10.1523/JNEUROSCI.2356-04.2005

Nelson, B. A., Gunton, K. B., Lasker, J. N., Nelson, L. B., & Drohan, L. A. (2008). The psychosocial aspects of strabismus in teenagers and adults and the impact of surgical correction. *Journal of American Association for Pediatric Ophthalmology and Strabismus*, *12*(1), 72–76.e1. https://doi.org/10.1016/j.jaapos.2007.08.006

Pasupathy, A., & Connor, C. E. (2002). Population coding of shape in area v4 [Number: 12 Publisher: Nature Publishing Group]. *Nature Neuroscience*, *5*(12), 1332–1338. https://doi.org/10.1038/972

Pasupathy, A., & Connor, C. E. (1999). Responses to contour features in macaque area v4 [Publisher: American Physiological Society]. *Journal of Neurophysiology*, *82*(5), 2490–2502. https://doi.org/10.1152/jn.1999.82.5.2490

Pasupathy, A., & Connor, C. E. (2001). Shape representation in area v4: Position-specific tuning for boundary conformation [Publisher: American Physiological Society]. *Journal of Neurophysiology*, *86*(5), 2505–2519. https://doi.org/10.1152/jn.2001.86.5.2505

Portilla, J., & Simoncelli, E. P. (2000). A parametric texture model based on joint statistics of complex wavelet coefficients. *International Journal of Computer Vision*, *40*(1), 49–70. https://doi.org/10.1023/A:1026553619983

Rahi, J. S., Logan, S., Timms, C., Russell-Eggitt, I., & Taylor, D. (2002). Risk, causes, and outcomes of visual impairment after loss of vision in the non-amblyopic eye: A population-based study. *The Lancet*, *360*(9333), 597–602. https://doi.org/10.1016/S0140-6736(02)09782-9

Rodman, H. R., Scalaidhe, S. P., & Gross, C. G. (1993). Response properties of neurons in temporal cortical visual areas of infant monkeys [Publisher: American Physiological Society]. *Journal of Neurophysiology*, *70*(3), 1115–1136. https://doi.org/10.1152/jn.1993.70.3.1115

Satterfield, D., Keltner, J. L., & Morrison, T. L. (1993). Psychosocial aspects of strabismus study. *Archives of Ophthalmology*, *111*(8), 1100–1105. https://doi.org/10.1001/archopht.1993.01090080096024

Serre, T., Oliva, A., & Poggio, T. (2007). A feedforward architecture accounts for rapid categorization [Publisher: Proceedings of the National Academy of Sciences]. *Proceedings of the National Academy of Sciences*, *104*(15), 6424–6429. https://doi.org/10.1073/pnas.0700622104

Springer, A. D., & Hendrickson, A. E. (2005). Development of the primate area of high acuity, 3: Temporal relationships between pit formation, retinal elongation and cone packing. *Visual Neuroscience*, *22*(2), 171–185. https://doi.org/10.1017/S095252380522206X

Usrey, W. M., & Alitto, H. J. (2015). Visual functions of the thalamus [_eprint: https://doi.org/10.1146/annurev-vision-082114-035920]. *Annual Review of Vision Science*, *1*(1), 351–371. https://doi.org/10.1146/annurev-vision-082114-035920

van de Graaf, E. S., van Kempen-du Saar, H., Looman, C. W. N., & Simonsz, H. J. (2010). Utility analysis of disability caused by amblyopia and/or strabismus in a population-based, historic cohort. *Graefe's Archive for Clinical and Experimental Ophthalmology*, *248*(12), 1803–1807. https://doi.org/10.1007/s00417-010-1457-z

Van Horn, S. C., Erişir, A., & Sherman, S. M. (2000). Relative distribution of synapses in the a-laminae of the lateral geniculate nucleus of the cat [_eprint: https://onlinelibrary.wiley.com/doi/pdf/10.1002 9861%2820000124%29416%3A4%3C509%3A%3AAID-CNE7%3E3.0.CO%3B2-H]. *Journal of Comparative Neurology*, *416*(4), 509–520. https://doi.org/10.1002/(SICI)1096-9861(20000124)416:4⟨509::AID-CNE7⟩3.0.CO;2-H

Victor, J. D., & Conte, M. M. (2012). Local image statistics: Maximum-entropy constructions and perceptual salience [Publisher: Optica Publishing Group]. *JOSA A*, *29*(7), 1313–1345. https://doi.org/10.1364/JOSAA.29.001313

Voss, P. (2013). Sensitive and critical periods in visual sensory deprivation. *Frontiers in Psychology*, *4*, 664. https://doi.org/10.3389/fpsyg.2013.00664

Webber, A. L., & Wood, J. (2005). Amblyopia: Prevalence, natural history, functional effects and treatment [Publisher: Taylor & Francis _eprint: https://doi.org/10.1111/j.1444-0938.2005.tb05102.x]. *Clinical and Experimental Optometry*, *88*(6), 365–375. https://doi.org/10.1111/j.1444-0938.2005.tb05102.x

Wiesel, T. N., & Hubel, D. H. (1963a). Effects of visual deprivation on morphology and physiology of cells in the cat's lateral geniculate body [Publisher: American Physiological Society]. *Journal of Neurophysiology*, *26*(6), 978–993. https://doi.org/10.1152/jn.1963.26.6.978

Wiesel, T. N., & Hubel, D. H. (1963b). Single-cell responses in striate cortex of kittens deprived of vision in one eye [Publisher: American Physiological Society]. *Journal of Neurophysiology*, *26*(6), 1003–1017. https://doi.org/10.1152/jn.1963.26.6.1003

Zhang, B., Smith, E. L., & Chino, Y. M. (2008). Postnatal development of onset transient responses in macaque v1 and v2 neurons [Publisher: American Physiological Society]. *Journal of Neurophysiology*, *100*(3), 1476–1487. https://doi.org/10.1152/jn.90446.2008

Zheng, J., Zhang, B., Bi, H., Maruko, I., Watanabe, I., Nakatsuka, C., Smith, E. L., & Chino, Y. M. (2007). Development of temporal response properties and contrast sensitivity of v1 and v2 neurons in macaque monkeys [Publisher: American Physiological Society]. *Journal of Neurophysiology*, *97*(6), 3905–3916. https://doi.org/10.1152/jn.01320.2006

Ziemba, C. M., Perez, R. K., Pai, J., Kelly, J. G., Hallum, L. E., Shooner, C., & Movshon, J. A. (2019). Laminar differences in responses to naturalistic texture in macaque v1 and v2 [Publisher: Society for Neuroscience Section: Research Articles]. *Journal of Neuroscience*, *39*(49), 9748–9756. https://doi.org/10.1523/JNEUROSCI.1743-19.2019

Zoccolan, D., Kouh, M., Poggio, T., & DiCarlo, J. J. (2007). Trade-off between object selectivity and tolerance in monkey inferotemporal cortex [Publisher: Society for Neuroscience Section: Articles]. *Journal of Neuroscience*, *27*(45), 12292–12307. https://doi.org/10.1523/JNEUROSCI.1897-07.2007